



Detailed Seismic Hazard, Disaggregation and Sensitivity Analysis for the Indo-Gangetic Basin

KETAN BAJAJ¹ and P. ANBAZHAGAN¹ 

Abstract—Seismic hazard in terms of peak ground acceleration (PGA) and spectral acceleration (SA) for the seismically active Indo-Gangetic Basin (IGB) has been computed using both a fault model and spatially smoothed-grid seismicity model. Seismicity parameters, viz. minimum magnitude, the maximum regional magnitude M_{\max} , mean seismic activity rate λ , the slope of the frequency–magnitude Gutenberg–Richter relationship, and the b -value ($b \ln(10)$), have been estimated spatially. The layered seismogenic source framework based on hypocentral depth distribution, i.e. 0–25, 25–70, and 70–180 km, for the smoothed-grid seismicity model has also been employed. The lowest λ_4 and λ_5 values for the IGB are 0.05 to 0.02 and 0.015 to 0.005, respectively, in the southern part of the IGB for hypocentral depth variation of 0–25 km. The IGB has a significant variation of seismicity in the entire stretch with noteworthy clustering in the northern side, which gradually decreases towards the south, and the spatial variability of the b -value and M_{\max} are 0.65–1.15 and 5.0–8.4 M_w , respectively. A ground-motion prediction equation has been selected and weighted by carrying out the efficacy test considering the past earthquakes. The disaggregation process is used for determining the spatial contribution of different magnitudes and distances for the whole IGB. Sensitivity analysis is used for examining the effect of various parameters. The PGA for the IGB varies from 0.06 to 0.54 g for 2% and 0.03 to 0.32 g for a 10% probability of exceedance in 50 years at bedrock condition. The developed average uniform hazard spectra in this study match well with the spectra derived from recorded ground motion. Based on the disaggregation process, dominant magnitude and distance are in the range of 4.7 to 6.0 M_w and 15 to 75 km, respectively, in the case of PGA and change to 5.5–7.2 M_w and 45 to 150 km in the case of 0.5 s and 5.8–7.5 M_w and 70 to 250 km in the case of 2.0 s. Sensitivity analysis suggested that increase in maximum magnitude and distance has an impact on hazard level over a longer period. This is the first time a detailed hazard analysis has been presented for the IGB.

Keywords: Indo-Gangetic basin, seismicity parameters, disaggregation, sensitivity analysis, hazard analysis.

1. Introduction

Due to earthquakes, destruction and vulnerability are increasing steadily in urban areas due to improper development and urbanization in a moderate or strong earthquake-prone area. Additionally, unrestrained spreading of cities and insufficient knowledge of seismic hazard may lead to a seismically unsafe scenario. Even a moderate earthquake leads to a catastrophic situation in areas with poor building and construction practices. One of the widely used and effective ways to reduce the disaster due to an earthquake is to predict the site-specific seismic hazard levels and appropriately upgrade the building design codes.

The Indo-Gangetic basin (IGB) was formed by lithospheric bending in response to an orogenic load and tectonic activity, which also resulted in extended sediment deposition (Fraser & DeCelles, 1992). The tectonic activity of the IGB has been discussed by various researchers (e.g. Sastri et al., 1971; Viridi, 1994). Based on the skewness of the fan surface, the sudden change in the alignment of the river, displacement of the Siwalik hills, etc., researchers (e.g. Kumar et al., 1996; Prakesh et al., 2000; Pati et al., 2015) have reported high neotectonic activity in the IGB. There are also a number of basement faults, namely the Bareilly, Moradabad, Lucknow, Patna, and Malda faults (Rao, 1973; Sastri et al. 1971). The southern part of the IGB shows E–W and ENE–WSW trending linear magnetic anomaly zones. Apart from faults, the IGB is also surrounded by important basement highs that are the Delhi–Hardwar ridge in the west, the Faridabad ridge in the middle, the Monghyr–Ghazipur ridge in the east, a poorly developed high in the Mirzapur–Ghazipur area, and smaller “highs” of Raxaul, Bahraich, and Puranpur. Additionally, the IGB is adjacent to one of the world most

Supplementary Information The online version contains supplementary material available at <https://doi.org/10.1007/s00024-021-02762-7>.

¹ Indian Institute of Science, Bangalore, Karnataka, India.

active tectonic regions, i.e. the Himalayas. Thus, any large-magnitude earthquake in the Himalayan region results in a catastrophe in the IGB (Bajaj & Anbazhagan, 2019a, 2019b). Hence in this study a seismic hazard map for the IGB at bedrock level has been developed both deterministically and probabilistically.

Various researchers have made attempts (e.g. Ashish et al., 2016; Nath & Thingbaijam, 2012; NDMA, 2010) at predicting the hazard value for entire India. However, most of the earlier studies did not account for uncertainties in the input variables of the hazard analysis. Additionally, significant improvements in the understanding of seismogenic sources and seismicity of the IGB demand a revision of the hazard map. Hence, in this study, all the basic elements [i.e. potential sources, seismicity parameters, and ground-motion prediction equations (GMPEs)] of hazard analysis have been studied extensively to reduce the uncertainty in hazard values. Various authors (Allen et al., 2004; Christova, 1992; Nath & Thingbaijam, 2012; Tsapanos, 2000) conclude that there is significant variation in the seismicity pattern and seismogenic source dynamics with hypocentral depth. Based on the hypocentral depth of the seismicity, three hypocentral depths, viz. 0–25, 25–70, and 70–180 km, have been considered. Seismicity parameters, i.e. minimum magnitude, the maximum regional magnitude M_{\max} , mean seismic activity rate λ , the slope of the frequency–magnitude Gutenberg–Richter relationship, and the β -value ($b \ln(10)$), for the IGB have been estimated spatially for the three hypocentral depths. GMPEs have been selected based on the log-likelihood (LLH) procedure proposed by Scherbaum et al. (2009) and Delavaud et al. (2009). Hazard values for the IGB at bedrock level are estimated using both deterministic and probabilistic approaches. Due to the absence of proper fault activity studies in the IGB, the hazard value has been calculated using both fault and spatially smoothed-grid seismicity models. The layered seismogenic source framework based on hypocentral depth distribution, i.e. 0–25, 25–70, and 70–180 km, for the smoothed-grid seismicity model has been employed. Hazard values have been estimated at 2% and 10% probability of exceedance in 50 years, i.e. for the return period of 2475 and 475 years, in the

case of probabilistic seismic hazard analysis (PSHA). A further disaggregation process has been used to determine the earthquake scenarios that drive the hazard at a given ground-motion level for the entire IGB. Finally, sensitivity analysis has been performed to examine the effect of various input parameters and understand the potential error in the hazard level estimation.

2. Seismicity of the Region

The tectonic features of the study area have been compiled from the Seismotectonic Atlas (SEISAT, 2010) published by the Geological Survey of India (GSI, 2000). For the preparation of the seismotectonic map, linear sources (faults and lineaments) are identified from SEISAT and published literature by considering a 500 km length around the IGB. Along with faults, demarcation of the Main Boundary Thrust (MBT), Main Central Thrust (MCT), and Himalayan Frontal Fault (HFF) has been done; the faults have been named and are given in Figure ES1 (a). These seismic sources have been collected from seismotectonic maps published by Gupta (2006), SEISAT (2010), Mukhopadhyay (2011), Nath and Thingbaijam (2012), and Kolathayar et al. (2012). These studies presented the seismotectonic map of the linear sources corresponding to the Himalayan and the Indian subcontinent. Linear sources in the IGB and the Himalaya have been mapped from Mukhopadhyay (2011) and used by Kolathayar et al. (2012). Most of the tectonic features close to the Western Himalaya, Kumaon Himalaya, Central/Nepal Himalaya, Eastern Himalaya, and Northeast Indian region have been mapped from Gupta (2006). In total, 387 seismic sources are identified, out of which 90 sources are lineaments, shear zones, neo-tectonic faults, and others. These 90 sources are also included in the hazard analysis. Among the remaining 297 sources, 76 active sources lie in the study area (distinguished in Figure ES1 (a) by naming from S1 to S76). These sources are considered separately and combined by allotting different weight factors (explained further).

The earthquake events database is collected from various agencies such as the National Earthquake

Information Centre (NEIC), International Seismological Centre, the Indian Meteorological Department (IMD), United States Geological Survey (USGS), Northern California Earthquake Data Center (NCEDC), and GSI. A total of 13,619 events have been compiled, which are in different magnitude scales such as local magnitude, surface wave magnitude, and body wave magnitudes. To achieve uniformity in magnitude, all the reported events are converted to moment magnitude (M_w) using relations given by Nath et al. (2017) for the South Asia data. The time and distance-windowing algorithms given by Gardner and Knopoff (1974) modified by Uhrhammer (1986) have been used to eliminate the dependent events. The sizes of the temporal and spatial windows are dependent on the mainshock magnitude and used as defined by Van Stiphout et al. (2012). Among the 13,619 events, about 29% were noticed as dependent events, i.e. 9707 events have been documented as the main shock for the IGB. The new up-to-date homogeneous catalog for the IGB has 9707 events with a period ranging from 1062 to 2017. The complete catalog contains 5244 events having moment magnitude less than 4 and 4464 events with $M_w \geq 4$. Further, the chi-square test is used to assess whether the declustered catalog exhibits Poisson's temporal behavior. Based on the result, the hypothesis that the declustered catalog is the realization of a Poisson process is not rejected at a significance level of 0.05. All the declustered earthquake events are given as Figure ES1 (b). To develop the seismotectonic map, declustered earthquake events are superimposed with the linear source map and given as Fig. 1. Figure 1 shows the seismotectonic map of the IGB with $M_w > 5.0$, and it can be observed from Fig. 1 that moderate earthquake events are denser near the MBT and MCT when compared to other parts.

3. Seismicity Parameter Estimation

One of the objectives of the study is to estimate the spatial variability in seismicity parameters, viz. maximum magnitude M_{max} , mean seismic activity rate λ , the slope of the frequency–magnitude Gutenberg–Richter relationship, and the β -value ($bln(10)$)

for the IGB. The whole seismic study area (shown in Fig. 1) is divided into the grid size of $0.01^\circ \times 0.01^\circ$ along the east–west and north–south directions, and seismicity parameters have been estimated. As per Anbazhagan et al. (2015a, 2019) and Khodaverdian et al. (2016), seismicity within 500 km around each grid should be considered in engineering analysis and design and hence utilized to estimate seismicity parameters in the present study. This is explained further using sensitivity analysis. The steps used in the more precise estimation of seismicity parameters are (1) the instrumental part of the catalog is accurately evaluated using the completeness test given by Stepp (1972), (2) time intervals with different completeness magnitudes are estimated using the methods given by Wiemer and Wyss (2000), (3) based on the time intervals determined in steps 1 and 2, different sub-catalogs are then provided using the whole earthquake catalog declustered by the method of Gardner and Knopoff (1974) modified by Uhrhammer (1986), and (4) the seismicity parameters β , λ , and M_{max} are computed by employing the maximum-likelihood procedure of Kijko and Sellevoll (1989, 1992), Kijko (2004), and Anbazhagan et al. (2015a, b).

Region-specific seismicity parameters need to be estimated by dividing the seismic catalog into sub-catalogs, and the completeness magnitudes for each subcatalog should also be determined. Firstly, the collected seismic data of the IGB has been scrutinized for its completeness by adopting Stepp's method (1972). The whole seismic catalog is divided into the magnitude bins of $4 \leq M_w < 5$, $5 \leq M_w < 6$, $6 \leq M_w < 7$, $7 \leq M_w < 8$, and $M_w \geq 8$ and in time intervals of 10 years. Based on the analysis of the whole catalog, it is found that the catalog is completed for 60, 80, 80, 90, and 100 years, respectively, for $4 \leq M_w < 5$, $5 \leq M_w < 6$, $6 \leq M_w < 7$, $7 \leq M_w < 8$, and $M_w \geq 8$ magnitude bins. The seismic catalog is defined as incomplete until 1956 and instrumented from 1957 to 2017, based on the completeness analysis for magnitude range $4 \leq M_w < 5$. Further, the period of completeness is evaluated for each grid by considering seismicity within a 500 km radius.

The magnitude of completeness (M_c) is defined as the lowest magnitude at which 100% of the

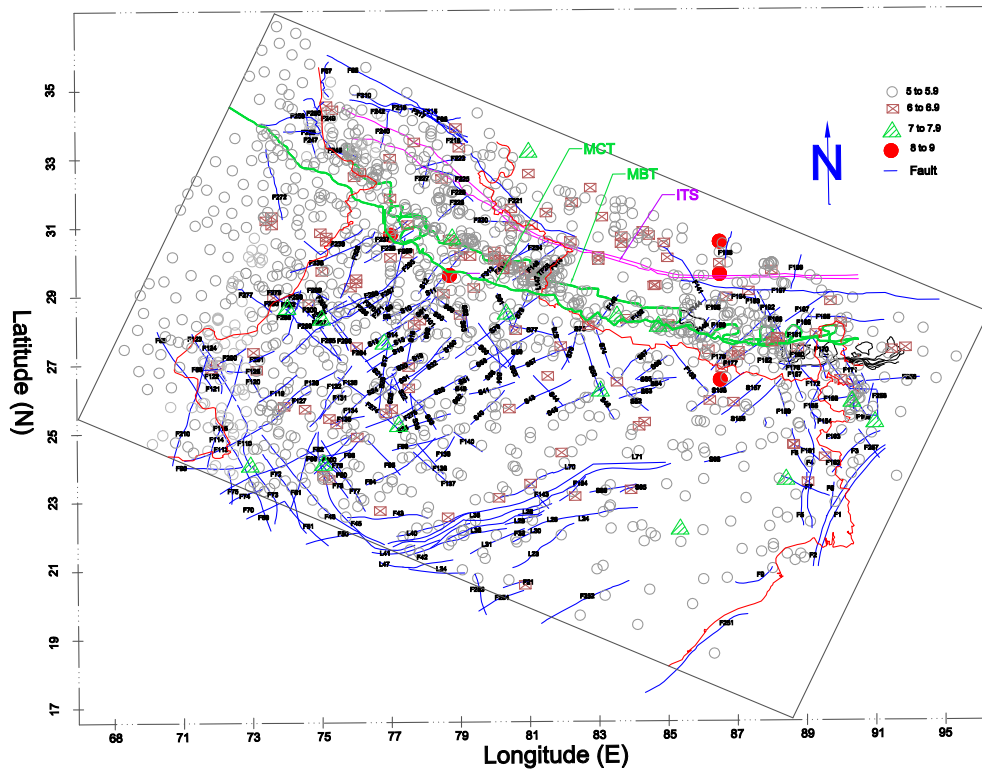


Figure 1
Seismotectonic map of the Indo-Gangetic Basin

earthquakes in a time volume are detected and derived for each grid. The temporal variation of M_c is evaluated using ZMAP software (Wiemer, 2001) by applying the maximum curvature method (MAXC). The cumulative number of instrumental earthquakes for the whole catalog and variation of M_c versus time period is plotted as Fig. 2. The slope of the cumulative number of earthquakes is constant at four time intervals. Hence, the completeness intervals for the mentioned grid point have been classified as 1957–1984, 1985–1995, 1996–2007, and 2008–2017 with a magnitude of uncertainty of 0.3, 0.3, 0.2, and 0.1, respectively.

Further, MAXC is used for determining the level of completeness at each interval (Wiemer & Wyss, 2000). As per MAXC, the maximum value of the first derivative of the frequency–magnitude curve is computed, and the magnitude attributed to the point of the maximum curvature is defined as M_c . In practice, this matches the magnitude bin with the

highest frequency of events in the non-cumulative frequency magnitude distribution. The main advantage of this method is that fewer events are needed, contrary to other approaches, to arrive at a stable result (Mignan et al., 2011). As for a few of the grid points, sub-catalogs have fewer seismic records due to the short duration of a time interval. Hence, MAXC is a robust method for calculating M_c for the IGB. The obtained results from MAXC were also compared with the entire magnitude range method (Woessner & Wiemer, 2005), and it is in good agreement with most of the grid points. This may be due to the minimum spatiotemporal heterogeneities in each sub-catalog. Plots of a cumulative number of earthquakes versus time and cumulative and non-cumulative frequency–magnitude distributions for the entire catalog are given in Fig. 3. M_c , as expected, decreases from 4.9 to 3.4; these values are further used as the magnitude threshold in the calculation of λ and β value for the IGB. Various authors (Allen

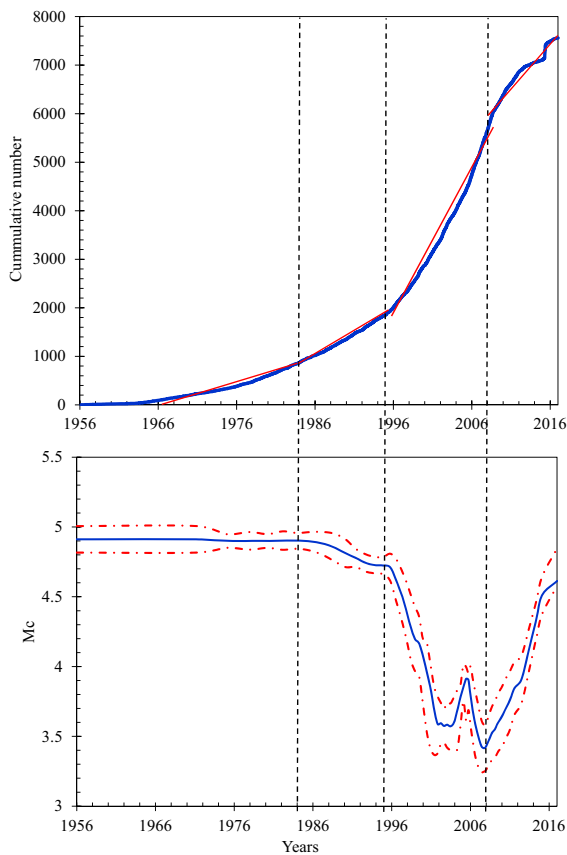


Figure 2

Cumulative number of instrumental earthquakes and variation of M_c with years

et al., 2004; Christova, 1992; Nath & Thingbaijam, 2012; Tsapanos, 2000) concluded that there is significant variation in the seismicity pattern and seismogenic source dynamics with hypocentral depth. Therefore, considering a single set of seismicity parameters over the entire depth range may result in incorrect estimation of hazard. Based on the hypocentral depth of the seismicity, three hypocentral depths, i.e. 0–25, 25–70, and 70–180 km, have been considered. The variation of a and b parameters of the Gutenberg–Richter relationship and M_c for the whole IGB for 0–25 km and 25–70 km is given as Fig. 4 and Figure 13, respectively. For the IGB, a and b parameters for the Gutenberg–Richter relationship vary from 3.8 to 5.4 and 0.78 to 1.13, respectively, for 0–25 km. a and b values change to 4.0 to 5.6 and 0.79 to 1.03, respectively, at 25–70 km hypocentral depth. Very few events are observed for hypocentral

depth 70–180 km and are only near the Punjab region. The calculated a and b values are 4.73 and 0.97, respectively, for hypocentral depth of 70–180 km. The a value is observed to be higher along the northern part of the IGB and decreases towards the southeastern part. There is significant variation in the b value in the Uttar Pradesh region; it changes from 0.75 in the northwestern part to 1.05 towards the southeastern part. As the northern part of the IGB is near the plate boundary, high a and low b values are observed (see Fig. 4). Along with the IGB, M_c (see Fig. 4c) varies from 4 to 5 M_w . A higher value of M_c is observed mostly near the northern part of Punjab and Haryana. However, for most of the IGB, the variation of M_c is between 4.4 and 4.6 M_w and between 4.6 and 4.8 M_w , respectively, at depths of 0–25 and 25–75 km. Hence, 4.5 M_w is considered as the magnitude of completeness for the whole IGB for predicting the hazard values.

Subcatalogs for each grid point are developed using the main shock event database and further used in the calculation of the seismicity parameters. Subsequently, Kijko and Sellevoll (MATLAB code HA2) (Kijko, 2010) is used in the calculation of the maximum magnitude M_{max} , mean seismic rate λ , and β value for of the frequency–magnitude Gutenberg–Richter relationship. The spatial variation of mean seismic rate λ for 4 M_w for the hypocentral depths of 0–25 km and 25–70 km is shown as Fig. 5a and b, respectively. Similarly, the distribution of λ for 5 M_w and 6 M_w is given as Figures 14 and 15, respectively. The highest seismicity is concentrated towards the northern part of the IGB near the Himalayan thrust. The seismicity is gradually decreased towards the southern parts of Bihar and Uttar Pradesh states of India. The values of λ_4 , λ_5 , and λ_6 vary from 0.02 to 0.210, 0.005 to 0.081, and 0.002 to 0.031, respectively, for hypocentral depth of 0–25 km. The lowest λ_4 and λ_5 values for the IGB are in the range of 0.05 to 0.02 and 0.015 to 0.005, respectively. The lowest values of λ_4 and λ_5 are observed in the southeastern part of the IGB. Observing the spatial variation of mean seismicity rate (Fig. 5), the IGB can be divided into three gross zones: (1) the high-seismicity zone, i.e. near the Himalayan thrust; (2) the medium-seismicity zone, i.e. the Ganga Plain; and (3) the low-seismicity zone, i.e. southeastern part of the IGB.

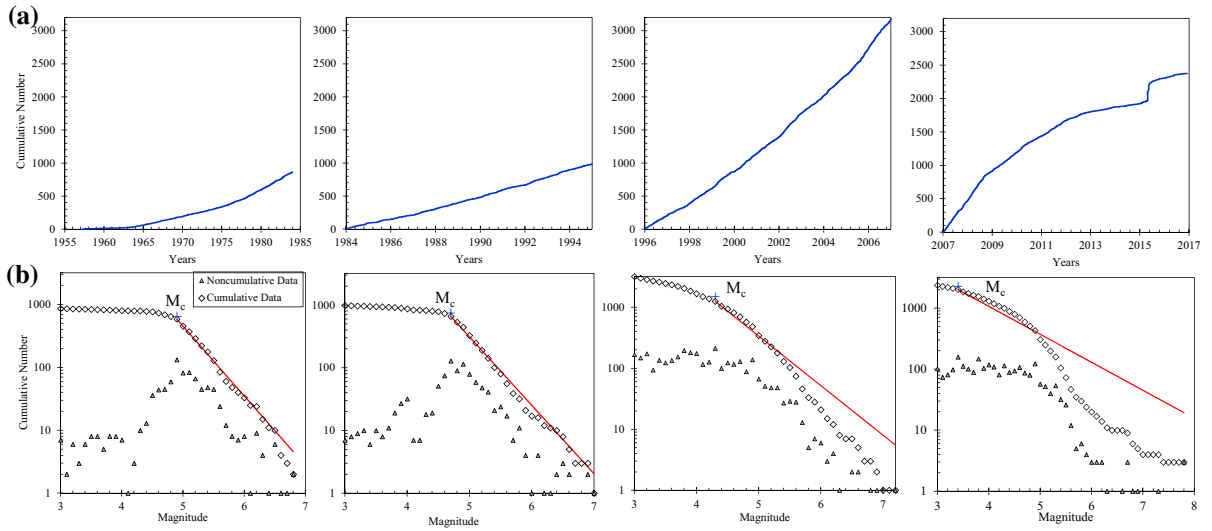


Figure 3

a Cumulative number of earthquakes versus time and b cumulative and noncumulative frequency–magnitude distributions for the different time periods

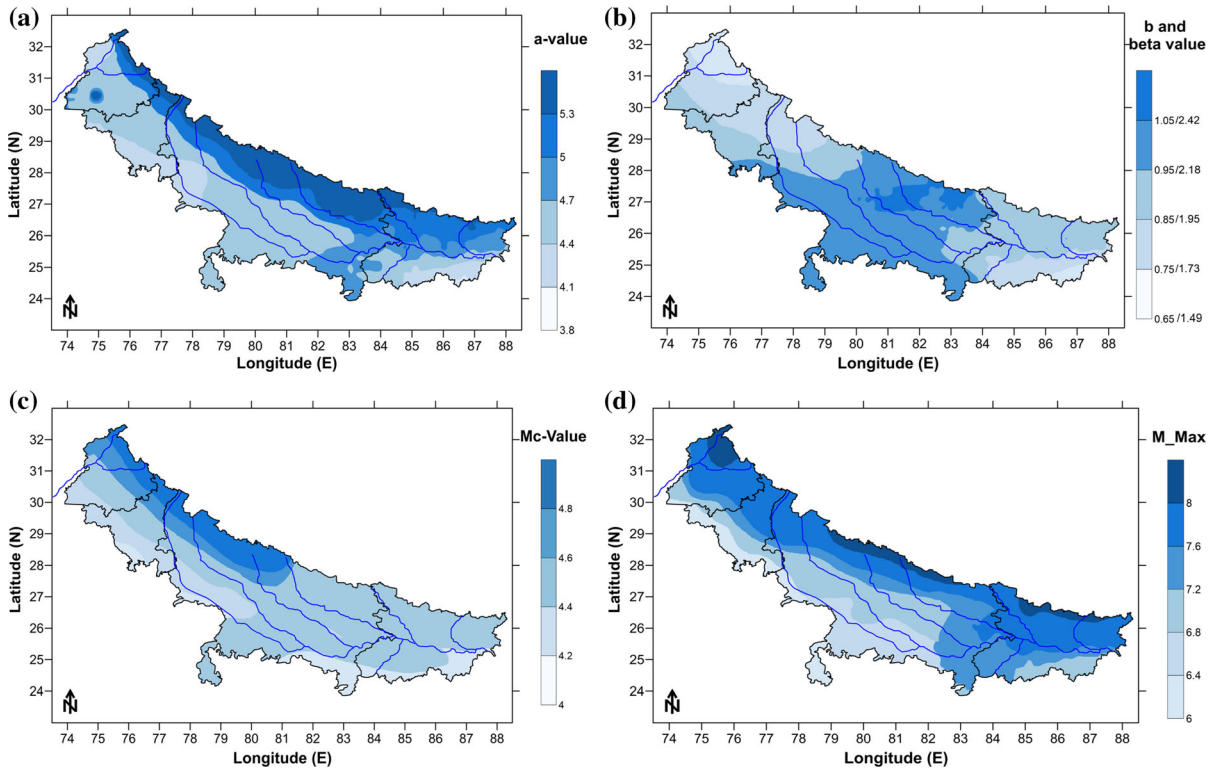


Figure 4

Spatial variation of the a and b parameters of the Gutenberg–Richter relationship, c M_c for hypocentral depth between 0 and 25 km, and d M_{max} calculated using all three methods

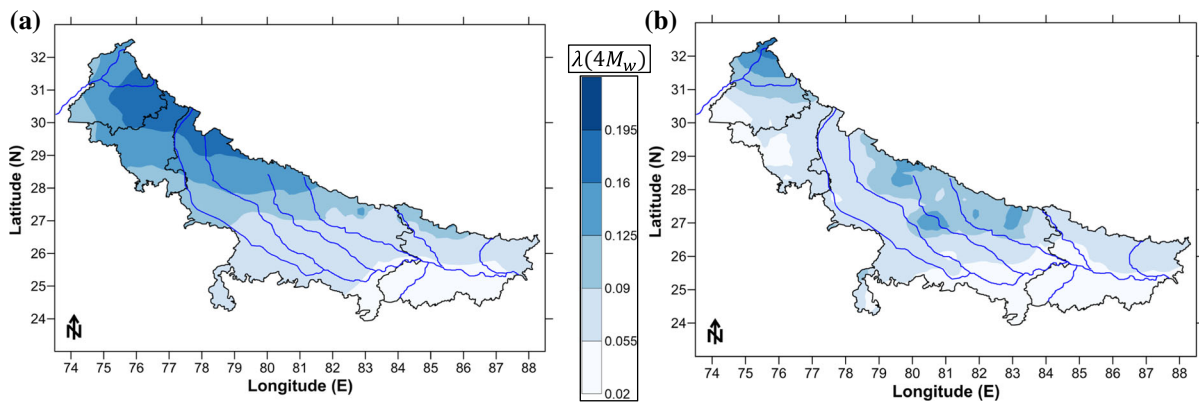


Figure 5

Spatial variation of mean seismic rate λ for $4 M_w$ at hypocentral depth regions of **a** 0–25 km and **b** 25–70 km

Based on the spatial variation of the seismicity parameter (see Figs. 4, 5), it can be concluded that significant variation of seismicity exists along the entire stretch of the IGB.

4. Maximum Magnitude Estimation and Selection of Ground-Motion Models

The maximum magnitude corresponding to each source has also been calculated using the regional rupture approach developed by Anbazhagan et al. (2015b). The regional rupture character is established by considering percentage fault rupture (PFR), which is the ratio of subsurface rupture length (RLD) to total fault length (TFL). PFR is further used to determine RLD and is further used for the estimation of M_{max} for each seismic source. RLD corresponding to the seismic source ($M_w \geq 4$) is calculated using a well-accepted correlation between RLD and M_w by Wells and Coppersmith (1994) from the maximum observed magnitude of each source. For estimating M_{max} from regional rupture characteristic, the whole study area is divided into two groups. One includes the seismic source with $4 \leq M_{obs}^{max} \leq 6$ (group 1) and the other with $M_{obs}^{max} > 6$ (group 2). This is done because of the large number of seismic sources and the activity of seismic source having $M_{obs}^{max} > 6$ is different from $M_{obs}^{max} < 6$. The regional rupture characteristics of both groups are given in Fig. 6. As there is a significant change in the TFL of the fault line and

the Himalayan thrust (MBT, MCT, and the Indus-Tsangpo Suture [ITS]), these are separated, and rupture characteristic is determined individually. PFR is established by considering minimum, maximum, and average PFR as shown in Table 1. The possible future rupture has been determined for the seismic study area based on the regional rupture character established considering past earthquakes and subsurface rupture length. Hence, the percentage fault rupture (PFR) for the future should be higher than the average regional trend and the maximum PFR in the region. Figure 6 has been carefully studied, and the trend of PFR with the total length for each bin (horizontal and vertical lines) are drawn. A horizontal line in Fig. 6 must be above the maximum PFR in each bin, i.e. above the maximum plotted PFR values of past earthquakes; it is considered the worst-case scenario of a particular bin. It is also necessary that the PER of the worst-case (the horizontal line) ratio of each bin should be more than unity, i.e. PFR of the worst-case scenario by average PER of the region. Table 1 shows the ratio of worst-case PFR used to estimate the maximum magnitude with the average PFR of the region. In Table 1, this ratio varies from 1.04 to 1.48. For group 2 (see Fig. 6), for TFL more than 300 km, the data points are scattered; hence increasing the maximum PFR may lead to an over-estimation of M_{max} . Therefore, for this particular bin, an increment has been done based on average PFR. The average PFR for the bin is 16.88 (% PFR). For the worst-case scenario, the qualitative increment

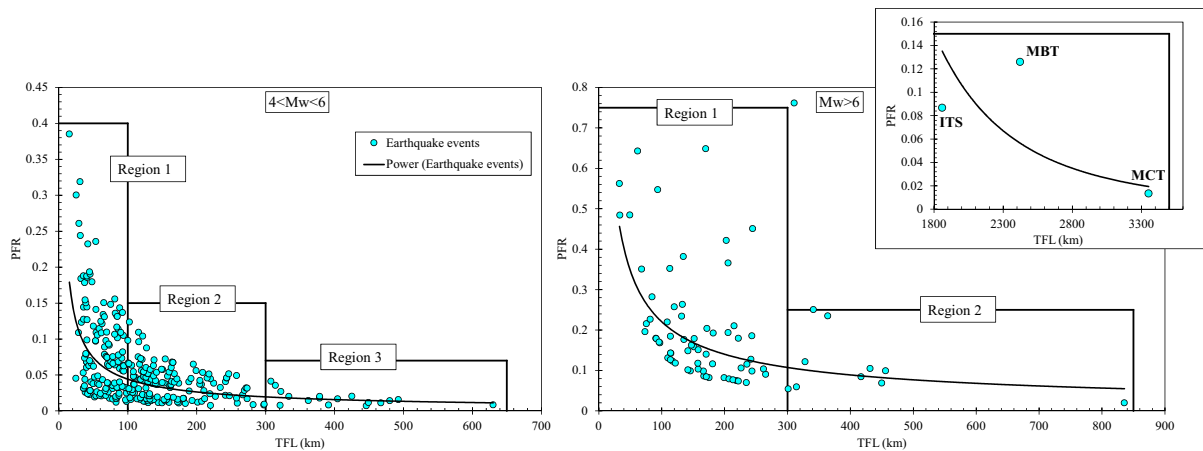


Figure 6

Estimation of regional rupture characteristics of subsurface rupture length in terms of total fault length for the whole IGB. The horizontal line shows the PFR for different distance bins given in Table 1

of 25% is considered for this particular bin (Anbazhagan et al., 2015a, b). Hence, the ratio of the worst-case scenario and average PFR (i.e. 25/16.88), which is 1.48, is considered as an incremental factor. However, estimating these factors requires a more scientific basis, so our study also focuses on the energy released by the earthquake in the region to arrive at these factors. The minimum and maximum values of M_{max} are calculated as 5.4 and 8.9, respectively, using the regional rupture character approach. Additionally, M_{max} is also calculated from conventional methods of increments of 0.5 in maximum observed magnitude (M_{obs}^{max}) based on “ b ” values of the Kijko method (Kijko, 2004). Budnitz et al. (1997) suggested an increment of 0.5 on maximum observed magnitude for the region having low b -value. M_{max} has been also estimated by adding a constant value of 0.5 to M_{obs}^{max} at each fault considering the conventional approach (Budnitz et al., 1997; NDMA, 2010). M_{max} estimated from Kijko (2004) is sensitive to the selected study area and seismicity parameters of a region (Anbazhagan et al., 2015a, b). As in the case of regional rupture characteristic, M_{max} is based on seismic source and rupture length; this can be considered more reliable than other approaches. As the proper fault mapping of the IGB is not available, M_{max} is estimated considering seismicity and seismic sources. For the final M_{max} determination, qualitative weight factors of 0.3, 0.3, and 0.4

have been assigned to the incremental method, the Kijko method, and the regional rupture method, respectively. Higher weight is given to the regional rupture approach as it accounts for rupture of the seismic source, which in turn depends upon the energy released for an event (Anbazhagan et al., 2015b). The final M_{max} varies from 5.0 M_w to 8.7 M_w by considering available faults. However, the final M_{max} values calculated corresponding to MBT, MCT, and ITS are 9.0 M_w , 8.5 M_w , and 9.0 M_w , respectively. Bilham and Ambraseys (2005) highlighted that the calculated slip rate in the Himalayan region in the central seismic gap is less than one third of the slip measured from GPS measurements. The difference in the slip can produce four events with $M_w > 8.5$ in the central seismic gap (Bilham and Ambraseys, 2005). Hence, considering 9.0 M_w as the maximum value might not be overestimation of M_{max} . The estimated maximum magnitude for each source in the study area is presented as electronic material in Table E1.

Like other seismicity parameters discussed above, spatial variation of M_{max} is also studied by considering all three approaches. The whole study area is divided into the grid size of 0.01×0.01 along east–west and north–south directions, and M_{max} is estimated for each grid. M_{max} from Kijko (2004) and the conventional approach is estimated by considering the earthquake events within 500 km around each

Table 1
Regional rupture characteristics of different distance bins for both groups

Length bin	PFR (% total)			PFR (% TFL) for worst scenario (WS)	Ratio of PFR for WS to maximum PFR
	Maximum	Minimum	Average		
$4 \leq M_{obs}^{max} \leq 6$ (group 1)					
< 100	38.51	1.19	8.59	40	1.04
100–300	12.34	0.75	3.84	15	1.21
> 300	4.12	0.70	1.73	7	1.71
$M_{obs}^{max} > 6$ (group 2)					
< 300	64.81	6.95	20.77	75	1.15
> 300	76.14	1.95	16.88	25*	1.48*
MBT, MCT, and ITS [^]					
-	15.51	2.88	9.54	15	1.13

* Calculated based on average

[^] MBT: Main Boundary thrust; MCT: Main Central Thrust; ITS: Indus–Tsangpo Suture

grid (explained above). As the regional rupture method developed by Anbazhagan et al. (2015b) considers only sources and not grids, M_{max} for each grid is assigned using the nearest source. Sources within a 500 km radius of each grid are determined, and the largest of all the faults is allotted as M_{max} for each grid. Similarly, the qualitative weight factors of 0.3, 0.3, and 0.4 have been assigned to the incremental method, Kijko method, and regional rupture method, respectively, for final M_{max} determination of each grid. The spatial variation of M_{max} along the IGB is given as Fig. 4d. M_{max} varies from 6 to 8.4 M_w along the entire stretch of the IGB. $M_w > 8$ is observed in the northern part of the IGB due to the presence of a plate boundary and high seismicity. All the seismicity parameters calculated in this section will be further used in determining the hazard value using the fault model and a spatially smoothed area source.

The selection of the ground-motion model is an important part in hazard analysis. Various researchers have analyzed the attenuation characteristics of the Himalayan region based on the available data. Region-specific GMPEs developed by Singh et al. (1996), Iyenger and Gosh (2004), Nath et al. (2005, 2009), Sharma and Bungum (2006), Das et al. (2006), Sharma et al. (2009), Gupta (2010), NDMA (2010), Anbazhagan et al. (2013), Nath et al. (2019), and Bajaj and Anbazhagan (2019b) are based on recorded as well as simulated earthquake data. For

determining the site-specific hazard values, a site-specific GMPE (Bajaj & Anbazhagan, 2019b) is developed for the IGB considering huge recorded and simulated data. As standard deviation is one of the most important parameters for estimating hazard value probabilistically, only BAN_19 values (see Table 2) were modeled using intra- and inter-event earthquake events variability, and not others. In addition to these GMPEs, there are several GMPEs developed for similar tectonic conditions, which can also apply to the Himalayan region. GMPEs developed elsewhere and relevant to the Himalayan regions include Abrahamson and Litehiser (1989), Youngs et al. (1997), Campbell (1997), Spudich et al. (1999), Atkinson and Boore (2003), Takahashi et al. (2004), Ambraseys et al. (2005), Kanno et al. (2006), Zhao et al. (2006), Campbell and Bozorgnia (2008), Idriss (2008), Boore and Atkinson (2008), Chiou and Youngs (2008), Abrahamson and Silva (2008), Lin and Lee (2008), Cauzzi and Faccioli (2008), Aghabarati and Tehranizadeh (2009), Akkar and Bommer (2010), Akkar et al. (2014), Bindi et al. (2014), Abrahamson and Silva (2014), Campbell and Bozorgnia (2014), Idriss (2014), Boore et al. (2014), and Zoha et al. (2016a, b, c). The list of GMPEs considered for predicting hazard values, along with their abbreviations, is given in Table 2. Details of all the GMPEs used along with their validity is given as an electronic supplement (See Table E2).

Table 2

Available GMPEs considered for seismic hazard analysis

S. no.	GMPE	Abbreviation
<i>Himalayan GMPE</i>		
1	Singh et al. (1996)	SI_96
2	Iyenger and Gosh (2005)	IYGO_05
3	Nath et al. (2005)	NA_05
4	Sharma and Bungum (2006)	SHBU_06
5	Das et al. (2006)	DA_06
6	Nath et al. (2009)	NA_09
7	Sharma et al. (2009)	SH_09
8	NDMA (2010)	NDMA_10
9	Gupta (2010)	GU_10
10	Anbazhagan et al. (2013)	AN_13
11	Bajaj and Anbazhagan (2019a, 2019b)	BAN_17
12	Nath et al. (2019a)	NA_19a
13	Nath et al. (2019b)	NA_19b
<i>Similar region GMPE</i>		
12	Abrahamson and Litehiser (1989)	ABLI_V_89
13	Abrahamson and Litehiser (1989)	ABLI_H_89
14	Youngs et al. (1997)	YO_97
15	Campbell (1997)	CAM_H_97
16	Campbell (1997)	CAM_V_97
17	Spudich et al. (1999)	SP_99
18	Atkinson and Boore (2003)	ATB_03
19	Takahashi et al. (2004)	TA_04
20	Ambraseys et al. (2005)	AMB_05
21	Kanno et al. (2006)	KA_06
22	Zhao et al. (2006)	ZH_06
23	Campbell and Bozorgnia (2008)	CABO_08
24	Idriss (2008)	ID_08
25	Boore and Atkinson (2008)	BOAT_08
26	Chiou and Youngs (2008)	CY_08
27	Abrahamson and Silva (2008)	ABSI_08
28	Lin and Lee (2008)	LL_08
29	Cauzzi and Faccioli (2008)	CAFA_08
30	Aghabarati and Tehranizadeh (2008, 2009)	AGTH_08_09_H
31	Aghabarati and Tehranizadeh (2008, 2009)	AGTH_08_09_V
32	Akkar and Bommer (2010)	AKBO_10
33	Akkar et al. (2014)	AK_14
34	Bindi et al. (2014)	BI_14
35	Abrahamson and Silva (2014)	ABSI_14
36	Boore et al. (2014)	BA_14
37	Campbell and Bozorgnia (2014)	CABO_14
38	Chiou and Youngs (2014)	CY_14
39	Idriss (2014)	ID_14
40	Zoha et al. (2016a); Subduction interface	ZH_16_SI
41	Zoha et al. (2016b); Subduction slab	ZH_16_SS
42	Zoha et al. (2016c); Crustal and upper mantle	ZH_16_CM

Forecasting the representative level of ground shaking from hazard analysis demands the appropriate selection of GMPEs (Bommer et al., 2010). The best-suited GMPE is selected considering the criteria proposed by Bommer et al. (2010) and by performing the efficacy test recommended by Scherbaum et al. (2009) and Delavaud et al. (2009). The information-theoretic approach developed by Scherbaum et al. (2009) has also been used. The efficacy test makes use of average sample log-likelihood (LLH) for the ranking purpose of the available GMPE of a particular study area. Hence, in the present study, an efficacy test has been carried out by considering the macroseismic intensity map of 1897 Shillong, 1934 Bihar–Nepal, 1991 Uttarkashi, 2005 Kashmir, and 2015 Nepal earthquakes. The intensity map is converted to a PGA map by using the PGA intensity equations proposed by Anbazhagan et al. (2016). Using these derived PGA values, LLH values and corresponding weights are calculated in accordance with Delavaud et al. (2009, 2012). The whole procedure is explained in Anbazhagan et al. (2015a). Observing the applicability and trends in GMPEs, the hypocentral distance is divided into three distance bins of 0–100 km, 100–300 km, and more than 300 km. As five different intensity maps are used for ranking of GMPEs and each has a different ranking, common GMPEs are selected for different distance bins, and average weights are assigned to the GMPEs. The selected GMPEs along with the weight for different distance bins are given in Table 3. The weight factor corresponding to a particular GMPE for different distance bins are further used in evaluating the seismic hazard values in terms of PGA and spectral acceleration (SA).

5. Seismic Hazard Analysis of IGB

Deterministic seismic hazard analysis (DSHA) and probabilistic seismic hazard analysis (PSHA) are widely used in determining the seismic hazard values of a site. In the present study, both DSHA and PSHA are used for determining the hazard value of the IGB in peak ground acceleration (PGA) and spectral acceleration (SA). A well-known PSHA algorithm developed by Cornell (1968), later improved by

Algermissen et al. (1982), is used in determining the hazard level using the fault model. The detailed procedure for hazard value estimation is explained in Anbazhagan et al. (2009). In house, MATLAB code has been developed to determine PGA and SA deterministically and probabilistically by considering the magnitude, source to site distance, and GMPE. Developed MATLAB code has been verified with the manual calculation at different cities in the IGB. The whole IGB is divided into a grid size of $0.01^\circ \times 0.01^\circ$ along the east–west and north–south directions, and hazard value is determined. Kriging interpolation technique has been used for the estimation of intermediate values of PGA for the development of the seismic hazard map for the whole IGB.

Hazard values are deterministically determined considering seismic sources with corresponding maximum magnitudes and systematically selected GMPEs having different weight factors. In total, 387 seismic sources have been found, which have experienced an earthquake magnitude of 4 and above and lie within 500 km around the IGB (shown in Fig. 1). These seismic sources are divided into three categories: (a) 76 sources inside the study area, (b) 221 sources outside the study area, (c) and 90 sources as

Table 3

Weights and ranking of GMPEs for different distance bins used in hazard analysis. Abbreviations are given in Table 2

GMPE	Weight	Ranking
<i>Distance ≤ 100</i>		
BAN_19	0.2858	1
ID_14	0.2424	2
ZH_16_SI	0.1912	3
AN_13	0.1386	4
NA_19a	0.0728	5
NA_09	0.0692	6
<i>100 < distance ≤ 300</i>		
BAN_19	0.2657	1
NA_19b	0.2015	2
ID_14	0.1715	3
ZH_16_CM	0.1589	4
ZH_16_SS	0.1058	5
KA_06	0.0966	6
<i>Distance > 300</i>		
BAN_19	0.6485	1
NDMA_10	0.3515	2

lineaments and (d) MBT, MCT, and ITS. Hazard values have been calculated based on two criteria: taking maximum of all and others using different weight factors. Weight factors for sources inside, outside, lineaments, and plate boundaries are 0.4, 0.25, 0.2, and 0.15, respectively. Figure 7a and b shows a DSHA map for the IGB using weight and maximum criteria. It can be seen from Fig. 7b that the middle portion of Uttar Pradesh has high hazard value which is due to the presence of the Great Boundary Fault and Moradabad Fault. High hazard values in Bihar and Haryana are due to the East Patna Fault and Ropar Fault, respectively. The presence of the Main Boundary Thrust and Jhelum Fault is the reason for high hazard value in the northwest part of Punjab.

PSHA consists of (a) potential earthquake source, (b) seismicity parameters, and (c) GMPEs. In a conventional PSHA approach, generally, a linear model that represents active faults in the IGB is used for defining earthquake source. A legitimate fault model contains detailed source characteristics, including both geomorphological and paleoseismological studies. The proper fault model is not defined for most regions of the IGB (see Fig. 1) due to the lack of detailed geologic and seismogenic studies. In the study area, limited analysis has been done on the earthquake catalog and activity of known faults. Hence, there may be several hidden active faults in the study area. Also, the seismic and geological data's quality and precision in different parts of the study area is unappealing. Hence, defining seismic hazard value based only on a fault-based model may be inconsistent. Thus, in addition to the fault-based model, hazard values are also defined using the smoothed-grid seismicity. The layered seismogenic source framework based on hypocentral depth distribution, i.e. 0–25, 25–70, and 70–180 km, for smoothed-grid seismicity model has been employed. For determining the hazard using the smoothed-grid seismicity, a single-area circular area source of 500 km radius is considered for the specified grid point. Similar to Khodaverdian et al. (2016), uniform β and M_{max} are considered over the areal source. However, λ varies in accordance with the observed earthquakes. Firstly, a more acceptable grid size of $0.01^\circ \times 0.01^\circ$ is considered, and the number of

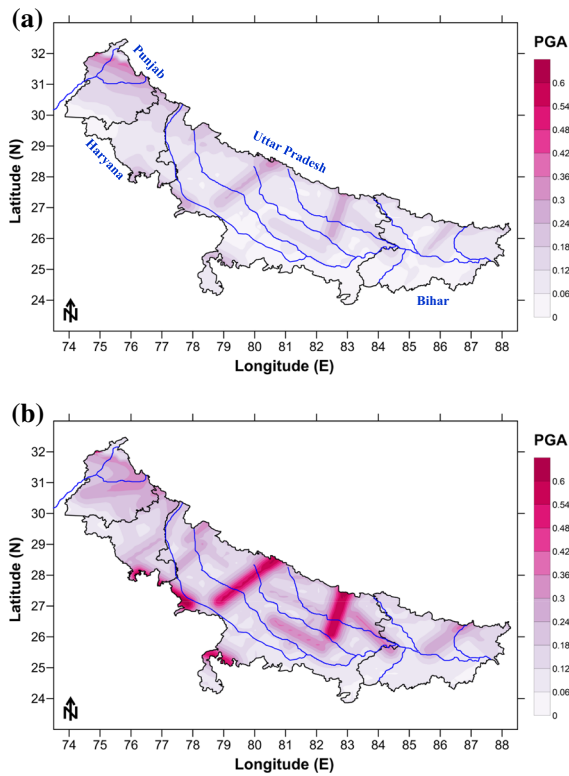


Figure 7

DSHA map for the IGB **a** using weight and **b** maximum criteria

earthquakes in each cell is computed considering the three hypocentral depth distributions. Like Frankel (1995), the 2D Gaussian function with a correlation distance of 40 km is applied. Further, using the calculated λ value from Kijko and Sellevoll (MATLAB code HA2) (Kijko, 2010), the spatially smoothed rate of occurrence is distributed.

The annual frequency at which ground motion at a site exceeds the chosen ground-motion (u_0) level using a total probability theorem can be computed as follows:

$$R(u > u_0) = \sum_i n_i(M_{min}) \times \int_{M_{min}}^{M_{max}} \int_r P[u > u_0 | m, r] p_i(m) p_i(r) dr dm, \quad (1)$$

in which $n_i(M_{min})$ is an annual seismic activity rate above the minimum magnitude M_{min} in a seismic source i (fault and each cell of the finer grid), $P[u > u_0 | m, r]$ is the conditional probability that an

earthquake of magnitude m at a distance r from the site generated ground motion u greater than the chosen level, and $p_i(m)$ and $p_i(r)$ are respectively the probability density functions for magnitude and distance between the point of source i and the site. The described methodology is further used in calculating the hazard values at bedrock level using the fault model and each cell as the source. PGA values are estimated for 2% and 10% probability of exceedance in 50 years, corresponding to a return period of 2475 and 475 years, respectively. Figure 8a and b show the PSHA map of the study area for 2475 years using the fault model and grid model. Hazard value calculated using a specially smoothed area source is underestimated near some faults; this could be due to the lack of fault activity in each grid (see Fig. 8). However, this is taken care of in a fault-based model. For example, in the northeast part of Bihar, the fault model is predicting a lower hazard value, but the areal model is predicting a higher value, which may be due to the spatial distribution of earthquake events and not associated with faults (see Fig. 8a, b). As explained above, in the absence of proper details of the faults in the IGB, the fault model is combined with the areal model, and hazard is calculated by giving a weight factor of 0.5 to each, as seen in Fig. 8c. Comparing to the DSHA map, the hazard value is less in central Uttar Pradesh, which may be due to less seismicity around the region. However, like DSHA, a high hazard value is observed in the northwest part of Punjab. Unlike DSHA, Haryana shows a significant hazard value which is due to the increased seismicity near the Delhi-Haridwar ridge. Similarly, the hazard level in Bihar is also significantly high as compared to the DSHA result.

The PGA for the IGB varies from 0.06 to 0.54 g for 2% probability in 50 years and 0.03 to 0.32 g in case of 10% probability in 50 years. Nath and Thingbaijam (2012) and NDMA (2010) developed the PSHA map for entire India, considering areal sources. Nath and Thingbaijam (2012) predicted the PGA of 0.08 to 0.3 g and 0.2 to 0.8 g for the seismic study area for a return period of 475 and 2475 years, respectively. As per NDMA (2010), PGA for the IGB for 2% and 10% probability of exceedance in 50 years, respectively, varies from 0.04 to 0.12 g and 0.03 to 0.05 g. Bhatia et al. (1999) predicted the PGA

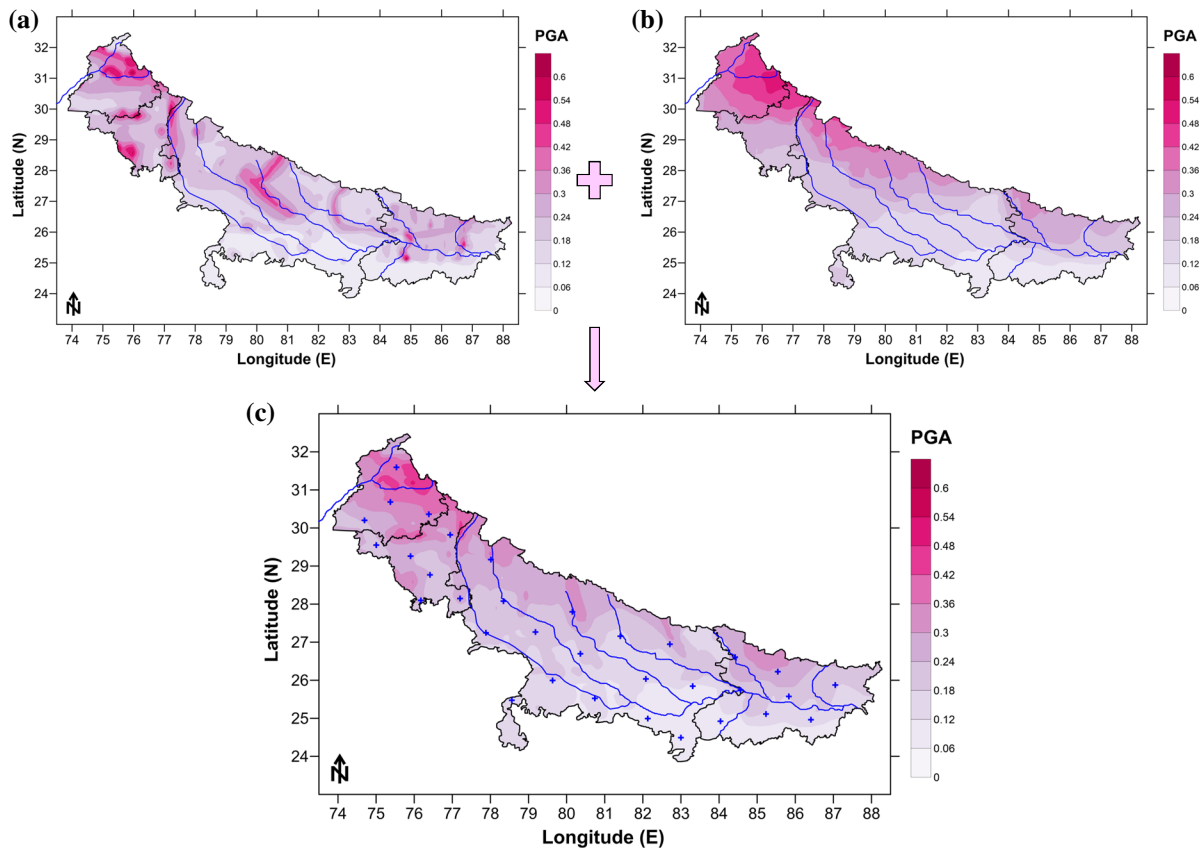


Figure 8

Two percent probability of exceedance in 50 years: **a** fault model, **b** areal model, and **c** combining both

value for the IGB for the return period of 475 years as 0.05 to 0.25 g. Rahman et al. (2018) predicted the hazard value for the IGB as 0.04–0.21 and 0.07–0.31 g for 10% and 2% probability of exceedance in 50 years, respectively. Nath et al. (2019) estimated the hazard value for Patna, Lucknow, and Varanasi for a return period of 475 and 2475 years. The bedrock PGA evaluated by Nath et al. (2019) is in the range of 0.138–0.149 g in Patna City, while it varies in the range 0.168–0.185 g in Lucknow and 0.091–0.109 g in the city of Varanasi. Hazard values determined by Rahman et al. (2018) are less compared to the present study, as their study only considered the seismicity near the Himalayan and Tibet region. The reasons for different values are the inclusion of various seismic sources and multiple models of activity rates. Further, in the present study, the updated version of the GMPEs with data-

supported weighing factors are used based on the qualitative analysis, i.e. LLH. Also, a new region-specific maximum magnitude estimation methodology is used in the determination of M_{max} for different seismic sources. The PGA value predicted in the present study is either higher or lower as compared to the previous work; this could be due to the use of updated seismicity, inclusion of depth-wise activity rate, region-specific determination of maximum magnitude, and selection of site-specific GMPEs. Further, in the present study, the epistemic uncertainty is being tested by including different GMPEs developed for the active crustal region.

Further site-specific uniform hazard spectra at bedrock level for 2% and 10% probability of exceedance at 50 years are developed at selected locations marked in Fig. 8c. Uniform hazard spectra at 5% damping for all selected locations are shown in

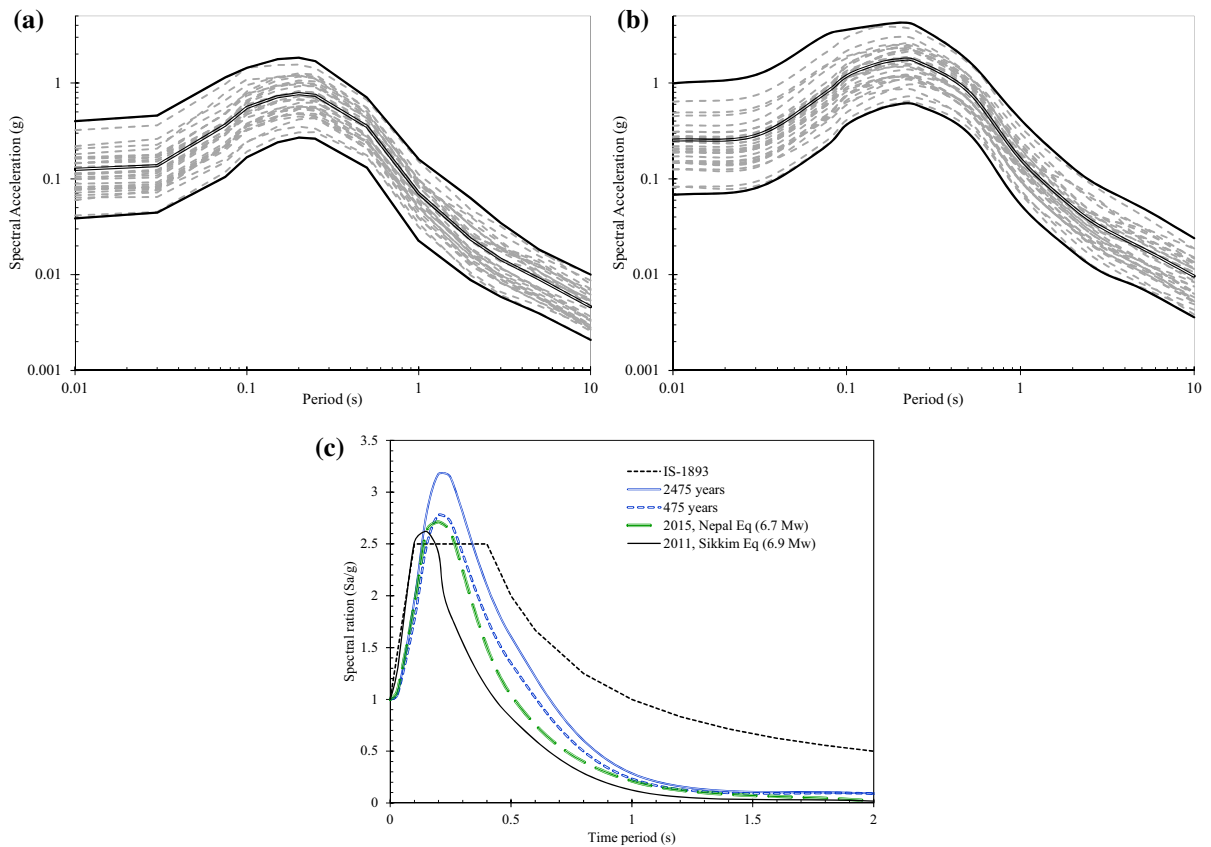


Figure 9

Uniform hazard spectra for **a** 10% and **b** 2% probability of exceedance in 50 years and **c** comparison of average normalized spectra at bedrock with IS-1893 and Nepal and Sikkim recorded ground motion at bedrock

Fig. 9a, b. The minimum, average, and maximum uniform hazard spectra (plotted as dark lines in Fig. 9) are also calculated for the IGB. Further, using the average response spectra at a different location in the study area, normalized hazard spectra are calculated for the return periods of 2475 and 475 years. This average normalized uniform hazard spectra of the IGB is compared with the design spectra given in the Indian standard code, i.e. IS-1893 (2016). Additionally, it is also compared with normalized spectra derived from recorded motions at bedrock level, i.e. 2015 Nepal ($6.7 M_w$) and 2011 Sikkim ($6.9 M_w$) earthquakes and given as Fig. 9c. The average normalized response spectra calculated in this study match well with the normalized spectra from recorded motions (Fig. 9c). A design spectrum from IS-1893 (2016) predicts a high value of spectral

acceleration at high periods as compared to normalized spectra from recorded data and developed for the IGB. As per Stein et al. (2012), for an interplate/intercontinental region like the IGB, hazard calculation based only on a fault model or areal source may lead to over- and underestimating the hazard value. PSHA carried out in this study considers both fault and a specially smoothed area source. Additionally, uncertainty in GMPE and source characterization is also considered. Hence, the hazard value predicted in this study is quite reliable.

6. Disaggregation and Sensitivity Analysis

Disaggregation in hazard analysis provides insights into the earthquake scenarios that drive the

hazard at a given ground-motion level. The disaggregation process differentiates the mean annual rate of exceedance (MRE) of specific ground motion at a site with respect to scenarios of given magnitude M , distance R , and the ground-motion error term ε . In short, it discloses which earthquake scenario (defined using M , R , and ε) controls the hazard at a site, which is very helpful in comparison with hazard curves. The dominant $M - R - \varepsilon$ group calculation using the disaggregation process helps to select the appropriate ground motion for nonlinear analysis for dynamic response of soil and structures. ε along with $M - R$ pair provide a better understanding of probabilistic ground-motion estimates and ground motions from deterministic scenarios (Harmsen, 1999). Detailed explanation about ε can be found in Hong and Goda (2006), Sousa and Costa (2008), and Barani et al. (2009).

The contribution of U to λ_u^0 (the mean annual rate) for a particular $M - R - \varepsilon$ pair at a site is given as

$$U(m_1 < M < m_2, r_1 < R < r_2, \varepsilon_1 < \varepsilon < \varepsilon_2 | u > u_0) = \frac{\sum_i n_i(m_{min}) \times \int_{m_1}^{m_2} \int_{r_1}^{r_2} f_{M,R}(m, r) f_\varepsilon(\varepsilon) P[u > u_0 | m, r, \varepsilon] dm dr d\varepsilon}{\lambda_u^0} \quad (2)$$

where $f_{M,R}(m, r)$ is the joint probability density function (PDF) of magnitude and distance; f_ε is the PDF for ground-motion error term ε ; $P[u > u_0 | m, r, \varepsilon]$ is the conditional probability of exceeding a particular ground-motion value u_0 of ground-motion parameter u for a given magnitude m , distance r , and ε standard deviations from predicted median ground motion.

In this study, disaggregation of hazard is studied for different sites for the return periods of 2475 and 475 years and for different periods using Eq. 2. Linear binning for magnitude, distance, and ε is used in this study with a bin size of $0.5 M_w$ over 20 km and an error of 0.5. Variation of magnitude, distance, and ε is $4 < M_w < 9$, $0 < R < 300$, and $-3 < \varepsilon < 3$, respectively. Typical disaggregation for 475- and 2475-year return periods at PGA and 1.0 s for grid point (30.73 N°, 76.76 E°) is given as Fig. 10. The $M - R - \varepsilon$ group changes from 4.8–38–1.22 in the case of PGA to 5.9–69–1.25 in the case of 1.0 s for grid point (30.73 N°, 76.76 E°) for the return period of 475 years. However, a significant change in ε is

observed while changing the return period from 475 to 2475 years. Significant hazard contribution is observed at a larger distance for the period of more than 1.0 s (see Fig. 10).

Similarly, the disaggregation process is carried out at each grid point in the study area using Eq. 2. Spatial variation of magnitude and distance for PGA value obtained from the disaggregation process for 2475 years is given as Fig. 11a, b, respectively. Dominant magnitude and distance are in the range of 4.7 to 6.0 and 15 to 75 km, respectively, in the case of PGA (see Fig. 11). A higher magnitude is obtained in the northwestern part of Punjab and northeastern part of Bihar state of India. This is due to the presence of an active fault and plate boundary. Additionally, the reason for the relatively large distance in the southern part of the IGB is the presence of neotectonic faults in the south and a plate boundary on the north side of it. However, the dominant values change to 5.5–7.2 and 45 to 150 in case of 0.5 s and 5.8–7.5 and 70 to 250 in case of 2.0 s for the entire stretch of the IGB. Based on the analysis, it can be concluded that for any nonlinear structural and soil analysis in the IGB, potential earthquake sources need to be considered up to 200 km and 75 km in the case of long and short vibration periods, respectively. Further, using these disaggregation result, sensitivity analysis has been done for the return periods of 475 and 2475 years.

PSHA consists of a number of input parameters having different uncertainties and impact on hazard value which is mainly reduced using the logic tree approach (Kulkarni et al., 1984; Marzocchi et al., 2015; Sokolov et al., 2017). To identify the effects of different parameters on hazard level, sensitivity analysis has been done for a return periods of 475 and 2475 years. The parameters used for sensitivity analysis are maximum magnitude, minimum magnitude, maximum distance, and GMPE. Figure 12 shows the typical result of sensitivity analysis for grid point (30.73 N°, 76.76 E°) for a 2% probability of exceedance in 50 years. Sensitivity analysis shows maximum magnitude (i.e. 6.5, 7, 7.5, and 8 M_w) has not much influence on hazard level for grid point (30.73 N°, 76.76 E°). The maximum magnitude changes with respect to the disaggregation process at different sites. A similar observation has been seen

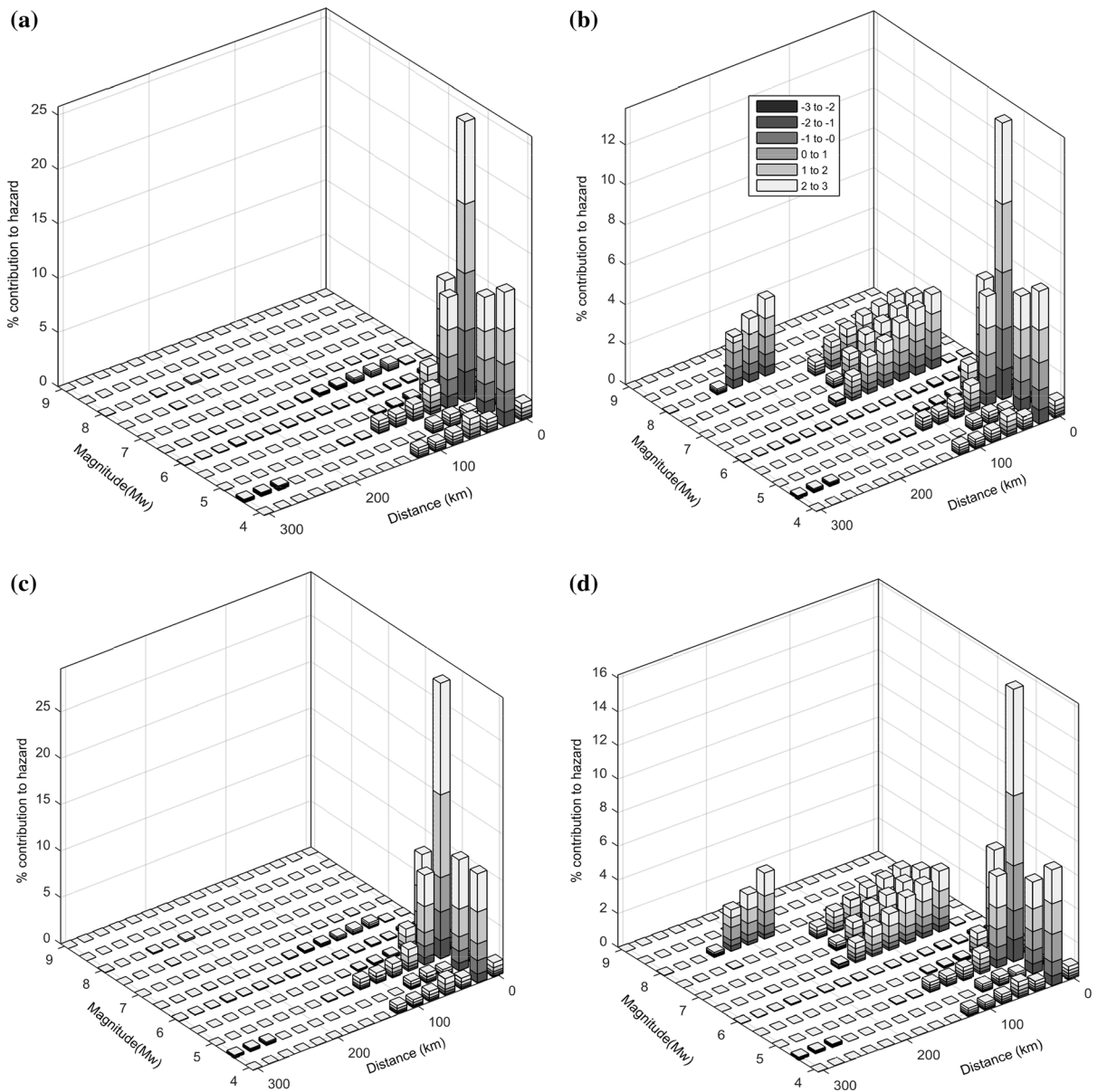


Figure 10

Disaggregation plot to obtain the joint $M - R - \epsilon$ pair for PGA at **a** 475 and **b** 2475 years and 1.0 s for **c** 475 and **d** 2475 years for grid point (30.73 N°, 76.76 E°)

from sensitivity analysis on a different part of the study area. In most of the cases, the hazard level at a higher magnitude (i.e. $M_w > 7.5$) is almost identical, as the occurrence is so unlikely that these magnitudes do not contribute much over lower time periods. However, there is a slight increase in hazard values over a larger period with the increase in magnitude. When the minimum magnitude changes from 4 to 5.0 M_w ,

there is an increase in hazard value at longer time periods. For example, in the case of grid point (30.73 N°, 76.76 E°) (see Fig. 12b), there is a 30 to 40% increase in hazard level for longer periods. Hence, a higher minimum magnitude may overestimate the hazard values for return periods of 475 and 2475 years. Based on the sensitivity analysis, the

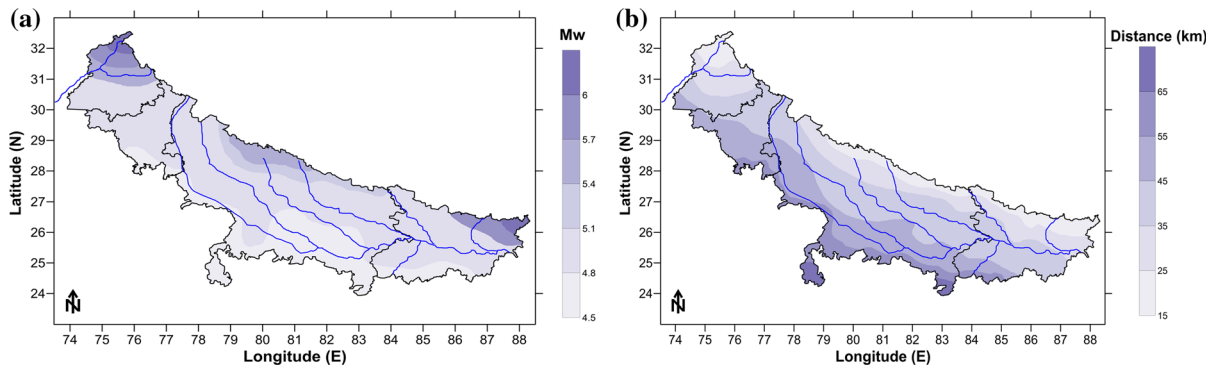


Figure 11

Spatial variation of **a** magnitude and **b** distance obtained from disaggregation process for 2475 years for PGA

minimum magnitude of $4.5 M_w$ can be recommended for any future hazard analysis in the IGB.

The maximum distance varies based on the disaggregation process at different sites. For example, at grid point ($30.73 N^\circ$, $76.76 E^\circ$), according to the disaggregation process, the scenario distance varies from 38 to 100 km for different time periods; hence, in sensitivity analysis, maximum distance varies from 20 to 500 km (see Fig. 12c). With the increase in the maximum distance at longer periods, there is an approximately 5 to 10% increase in hazard level in the case of both 475- and 2475-year return periods. This shows that maximum distance has no significant influence at shorter periods and little or negligible influence for longer periods. Based on sensitivity analysis at different locations in SA, it can be concluded that a minimum of 300 to 500 km needs to be used as the maximum distance for any hazard analysis study in the IGB, and this is in agreement with the disaggregation results. Further, the influence of all the GMPEs selected based on the LLH process is tested by employing them individually or combined using the weight factor calculated previously. Based on the analysis, it is seen that BA_19 and ID_14 have yielded a higher hazard value as compared to others at different time periods. The analysis shows that the combined GMPEs' trend lies almost in the middle range, which is used in determining the hazard values in present SA.

7. Conclusions

Seismic hazard values in terms of peak ground acceleration and spectral acceleration for the IGB have been computed considering both a fault model and a spatially smoothed area source. Seismicity parameters i.e. maximum regional magnitude M_{max} , mean seismic activity rate λ , the slope of the frequency–magnitude Gutenberg–Richter relationship, and the β -value ($b \ln(10)$) for the IGB have been estimated. Based on the analysis, it is seen that on average, the seismic catalog is incomplete until 1956 for the IGB. For the IGB, a and b parameters and M_c spatially vary from 3.8 to 5.6, 0.65 to 1.15, and 4 to 5 M_w , respectively. The lower range of λ_4 and λ_5 for the IGB are observed on the southern side, and the values are in the range of 0.1 to 0.6 and 0.01 to 0.05, respectively. The highest seismicity is concentrated towards the Himalayan thrust, which is the northern part of the IGB. The seismicity gradually decreases towards the southern part of Bihar and the Uttar Pradesh state of India. M_{max} has been estimated considering regional rupture characteristics; the Kijko method and conventional method are used, and the final value is calculated based on the weighted average. Spatial variability of M_{max} is 6.0 to 8.4 M_w , and the higher value is observed in the northern part of the IGB. The ground-motion prediction equation

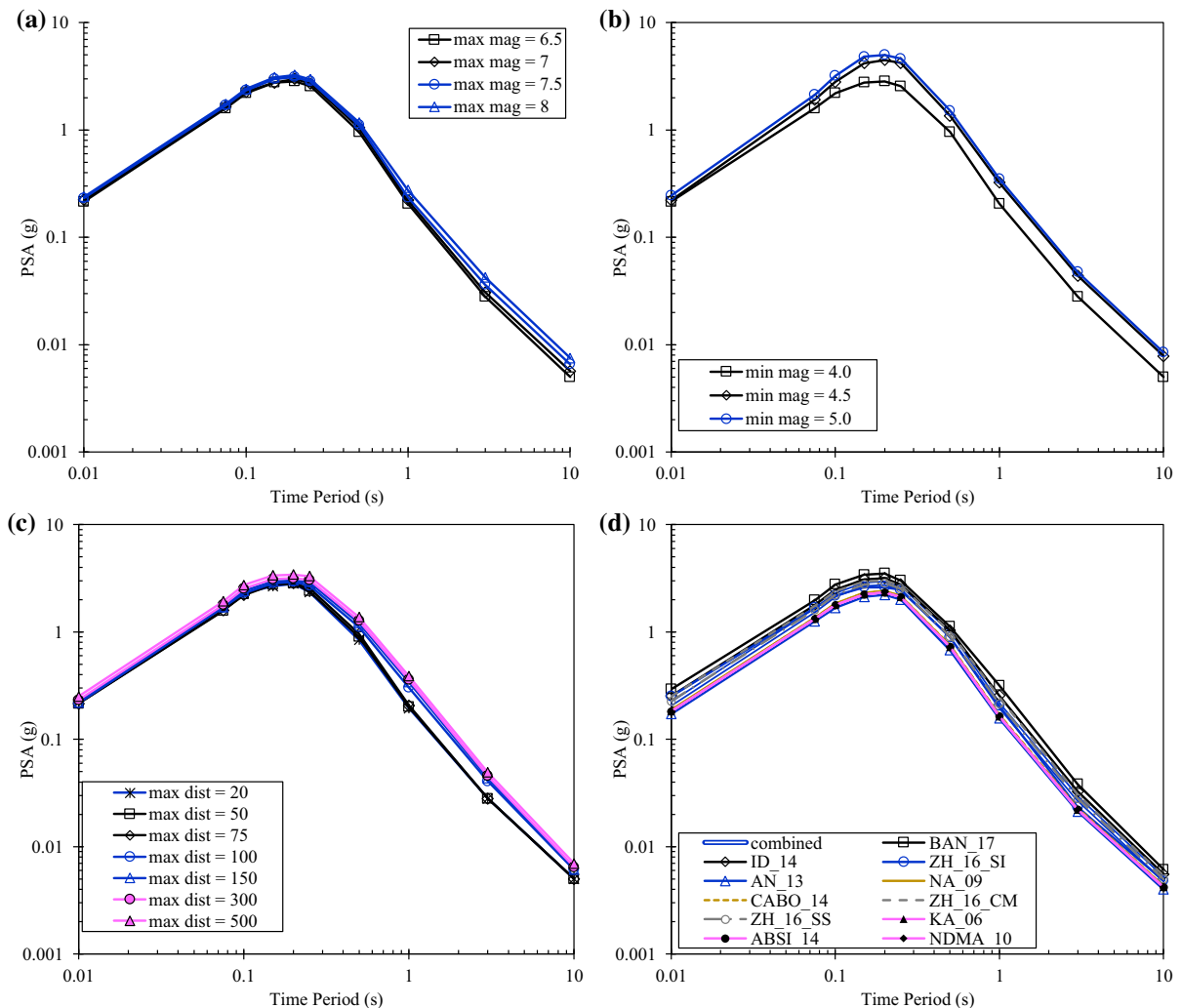


Figure 12

Sensitivity analysis for grid point (30.73 N°, 76.76 E°) for a return period of 2475 years considering input parameters as **a** maximum magnitude, **b** minimum magnitude, **c** maximum distance, and **d** GMPE

has been selected and weighted by carrying out the efficacy test considering the past earthquakes. Considering the seismicity parameters, GMPEs, and sources, the hazard value of the IGB is estimated both deterministically and probabilistically. The PGA for the IGB varies from 0.06 to 0.54 g for 2% probability in 50 years and 0.03 to 0.32 g in case of 10% probability in 50 years. The average uniform hazard spectra developed in this study match well with the spectra derived from recorded ground motion. The disaggregation process is used to determine the contribution of different magnitudes and distances, and sensitivity analysis is used for examining the effect of

various parameters. Based on the disaggregation process, the dominant magnitude and distance are in the range of 4.7–6.0 and 15–75 km, respectively, in the case of PGA and change to 5.5–7.2 and 45–150 in the case of 0.5 s and 5.8–7.5 and 70–250 in case of 2.0 s. Sensitivity analysis suggested that increase in maximum magnitude and distance has an impact on hazard level over a longer period.

Acknowledgements

The authors thank the Science and Engineering Research Board (SERB) of the Department of Science and Technology (DST), India for funding the project titled “Measurement of shear wave

velocity at deep soil sites and site response studies”, Ref: SERB/F/162/2015-2016.

Appendix

See Figs. 13, 14, and 15.

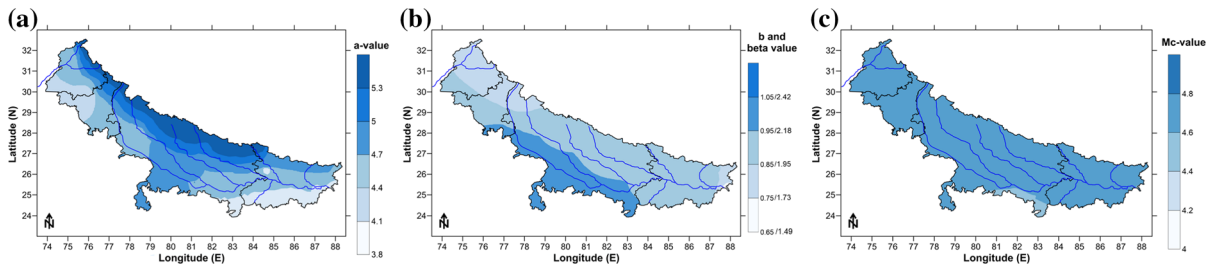


Figure 13
Distribution of **a** **b** parameters of Gutenberg–Richter relationship, **c** M_c for hypocentral depth between 25 and 70 km

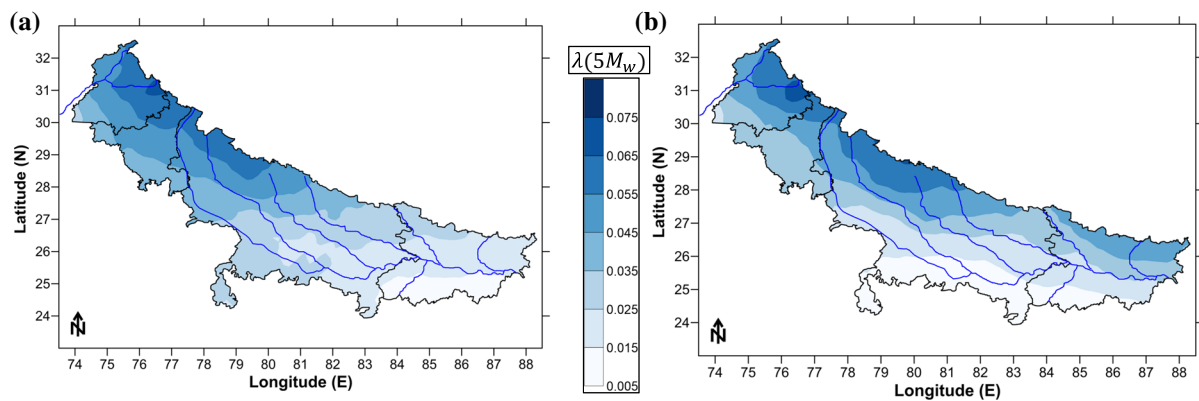


Figure 14
Spatial variation of mean seismic rate λ for $5 M_w$ at hypocentral depth regions **a** 0–25 km and **b** 25–70 km

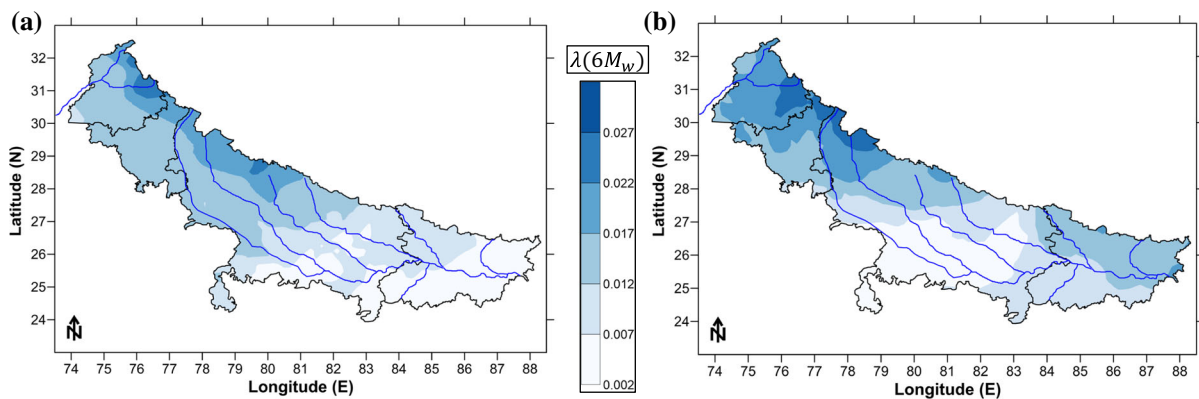


Figure 15
Spatial variation of mean seismic rate λ for $6 M_w$ at hypocentral depth regions **a** 0–25 km and **b** 25–70 km

Publisher's Note Springer Nature remains neutral with regard to jurisdictional claims in published maps and institutional affiliations.

REFERENCES

- Abrahamson, N. A., & Litehiser, J. J. (1989). Attenuation of vertical peak accelerations. *Bulletin of the Seismological Society of America*, 79, 549–580.
- Abrahamson, N., & Silva, W. (2008). Summary of the Abrahamson & Silva NGA Ground-Motion Relations. *Earthquake Spectra*, 24, 67–97.
- Abrahamson NA, Silva WJ, Kamai R (2014) Summary of the ASK14 ground-motion relation for active crustal regions. *Earthquake Spectra*. <https://doi.org/10.1193/070913EQS198M>.
- Aghabarati, H., & Tehranizadeh, . (2009). Near-source ground motion attenuation relationship for PGA and PSA of vertical and horizontal components. *Bulletin of Earthquake Engineering*, 7, 609–635.
- Akkar, S., & Bommer, J. J. (2010). Empirical equations for the prediction of PGA, PGV and spectral acceleration in Europe, the Mediterranean region and the Middle East. *Seismological Research Letters*, 81(195), 206.
- Akkar, S., Sandikkaya, M. A., & Bommer, J. J. (2014). Empirical ground motion models for point and extended-source crustal earthquake scenarios in Europe and the Middle East. *Bulletin of Earthquake Engineering*, 12, 359–387.
- Algermissen, S. T., Perkins, D. M., Thenhaus, P. C., Hanson, S. L., Bender, & B. L. (1982) Probabilistic estimates of maximum acceleration and velocity in rock in the contiguous United States. Open-File Report 82–1033. U.S. Geological Survey, Washington, DC, p 99
- Allen, T. I., Gibson, G., Brown, A., & Cull, J. P. (2004). Depth variation of seismic source scaling relations: Implications for earthquake hazard in southeastern Australia. *Tectonophysics*, 390, 5–24.
- Ambraseys, N., Douglas, J. S., Sarma, K., & Smit, P. M. (2005). Equation for the estimation of strong ground motions from shallow crustal earthquakes using data from Europe and the Middle East: horizontal peak ground acceleration and the spectral acceleration. *Bulletin of Earthquake Engineering*, 3, 1–53.
- Anbazhagan, P., Vinod, J. S., & Sitharam, T. G. (2009). Probabilistic seismic hazard analysis for Bangalore. *Natural Hazards*, 48, 145–166.
- Anbazhagan, P., Kumar, A., & Sitharam, T. G. (2013). Ground motion prediction equation considering combined data set of recorded and simulated ground motions. *Soil Dynamics and Earthquake Engineering*, 53, 92–108.
- Anbazhagan, P., Bajaj, K., & Patel, S. (2015a). Seismic hazard maps and spectrum for Patna considering region-specific seismotectonic parameters. *Natural Hazards*. <https://doi.org/10.1007/s11069-015-1764-0>
- Anbazhagan, P., Bajaj, K., Moustafa, S. S. R., & Al-Arifi, N. S. N. (2015b). Maximum magnitude estimation considering the regional rupture character. *Journal of Seismology*. <https://doi.org/10.1007/s10950-015-9488-x>
- Anbazhagan, P., Bajaj, K., Moustafa, S. S. R., & Al-Arifi, N. S. N. (2016). Relationship between Intensity and Recorded Ground-Motion and Spectral Parameters for the Himalayan Region. *Bulletin of the Seismological Society of America*. <https://doi.org/10.1785/0120150342>
- Anbazhagan, P., Bajaj, K., Matharu, K., Moustafa, S. S. R., & Al-Arifi, N. S. N. (2019). Probabilistic seismic hazard analysis using logic tree approach - Patna District (India). *Natural Hazards and Earth Systems Sciences*, 19, 2097–2115.
- Ashish, L. C., Parvez, I. A., et al. (2016). Probabilistic earthquake hazard assessment for Peninsular India. *Journal of Seismology*, 20, 629. <https://doi.org/10.1007/s10950-015-9548-2>
- Atkinson, G. M., & Boore, D. M. (2003). Empirical ground-motion relations for subduction-zone earthquakes and their applications to Cascadian and other regions. *Bulletin of the Seismological Society of America*, 93, 1703–1717.
- Bajaj, K., & Anbazhagan, P. (2019a). Comprehensive Amplification Estimation of the Indo Gangetic Basin Deep Soil Sites in the Seismically Active Area. *Soil Dynamics and Earthquake Engineering*. <https://doi.org/10.1016/j.soildyn.2019.105855>
- Bajaj, K., & Anbazhagan, P. (2019b). Regional stochastic GMPE with available recorded data for active region – Application to the Himalayan region. *Soil Dynamics and Earthquake Engineering*. <https://doi.org/10.1016/j.soildyn.2019.105825>
- Barani, S., Spallarossa, D., & Bazzurro, P. (2009). Disaggregation of Probabilistic Ground-Motion Hazard in Italy. *Bulletin of the Seismological Society of America*. <https://doi.org/10.1785/0120080348>
- Bhatia, S. C., Ravi, M. K., & Gupta, H. K. (1999). A probabilistic seismic hazard map of India and adjoining regions. *Annali Di Geofisica*, 42, 1153–1164.
- Bilham, R., & Ambraseys, N. (2004). Apparent Himalayan slip deficit from the summation of seismic moments for Himalayan earthquakes, 1500–2000. *Current Science*, 88(10), 1658–1663.
- Bindi, D., Massa, M., Luzi, L., Ameri, G., Pacor, F., Puglia, R., & Augliera, P. (2014). Pan-European ground motion prediction equations for the average horizontal component of PGA, PGV, and 5%-damped PSA at spectral periods up to 3.0 S using the RESORCE dataset. *Bulletin of Earthquake Engineering*, 12, 391–430.
- Bommer, J. J., Douglas, J., Scherbaum, F., Cotton, F., Bungum, H., & Fäh D, . (2010). On the selection of ground-motion prediction equations for seismic hazard analysis. *Seismological Research Letters*, 81(5), 783–793.
- Boore, D. M., & Atkinson, G. M. (2008). Ground-Motion Prediction Equations for the average horizontal component of PGA, PGV and 5% damped PSA at spectral periods between 0.01 and 10.0 s. *Earthquake Spectra*, 24(1), 99–138.
- Boore, D. M., Stewart, J. P., Seyhan, E., & Atkinson, G. M. (2014). NGAWest 2 equations for predicting PGA, PGV, and 5%-damped PSA for shallow crustal earthquakes. *Earthquake Spectra*. <https://doi.org/10.1193/070113EQS184M>
- Budnitz, R. J., Apostolakis, G., Boore, D. M., Cluff, L. S., Coppersmith, K. J., Cornell, C. A., & Morris, P. A. (1997). recommendations for PSHA: guidance on uncertainty and use of experts. NUREG/CR-6372, vol 1. US Nuclear Regulatory Commission, Washington, DC.
- Campbell, K. W. (1997). Empirical near-source attenuation relationships for horizontal and vertical components of peak ground acceleration, peak ground velocity and pseudo-absolute acceleration response spectra. *Seismological Research Letters*, 68(1), 154–179.

- Campbell, K. W., & Bozorgnia, Y. (2008). NGA ground motion model for the geometric mean horizontal component of PGA, PGV, PGD and 5 % damped linear elastic response spectra for period ranging from 0.01 to 10 s. *Earthquake Spectra*, 24, 139–171.
- Campbell, K. W., & Bozorgnia, Y. (2014). NGA-West 2 ground motion model for the average horizontal components of PGA, PGV, and 5%- damped linear acceleration response spectra. *Earthquake Spectra*. <https://doi.org/10.1193/062913EQS175M>
- Cauzzi, C., & Faccioli, E. (2008). Broadband (0.05 to 20s) prediction of displacement response spectra based on worldwide digital records. *Journal of Seismology*, 12(4), 453–475.
- Chiou, B. S. J., & Youngs, R. R. (2008). An NGA Model for the average horizontal component of peak ground motion and response spectra. *Earthquake Spectra Doi*, 10(1193/1), 2894832.
- Christova, C. (1992). Seismicity depth pattern, seismic energy and b value depth variation in the Hellenic Wadati-Benioff zone. *Physics of the Earth and Planetary Interiors*, 72, 38–48.
- Cornell, C. A. (1968). Engineering seismic risk analysis. *Bulletin of the Seismological Society of America*, 58, 1583–1606.
- Das, S., Gupta, I. D., & Gupta, V. K. (2006). A probabilistic seismic hazard analysis of Northeast India. *Earthquake Spectra*, 22, 1–27.
- Delavaud, E., Scherbaum, F., Kuehn, N., & Riggelsen, C. (2009). Information-theoretic selection of ground-motion prediction equations for seismic hazard analysis: An applicability study using Californian data. *Bulletin of the Seismological Society of America*, 99, 3248–3263.
- Delavaud, E., Scherbaum, F., Kuehn, N., & Allen, T. (2012). Testing the global applicability of ground-motion prediction equations for active shallow crustal regions. *Bulletin of the Seismological Society of America*, 102(2), 702–721.
- Frankel, A. (1995). Mapping seismic hazard in the central and eastern United States. *Seismological Research Letters*, 66, 8–21.
- Fraser, G. S., & DeCelles, G. (1992). Geomorphic controls on sediment accumulation at margins of foreland basins. *Basin Research*, 4, 233–252.
- Gardner, J. K., & Knopoff, L. (1974). Is the sequence of earthquakes in southern California, with aftershocks removed, poissonian? *Bulletin of the Seismological Society of America*, 64(5), 1363–1367.
- GSI. (2000). Eastern Nepal Himalaya and Indo-Gangetic Plains of Bihar. In P. L. Narula, S. K. Acharyya, & J. Banerjee (Eds.), *Seismotectonics Atlas of India and its environs* (pp. 26–27). Geological Survey of India.
- Gupta, I. D. (2006). Delineation of probable seismic sources in India and neighborhood by a comprehensive analysis of seismotectonic characteristics of the region. *Soil Dynamics and Earthquake Engineering*, 26, 766–790.
- Gupta, I. D. (2010). Response spectral attenuation relations for inslab earthquakes in Indo-Burmese subduction zone. *Soil Dynamics and Earthquake Engineering*, 30, 368–377.
- Harmsen, S., Perkins, D., & Frankel, A. (1999). Deaggregation of probabilistic ground motions in the central and eastern United States. *Bulletin of the Seismological Society of America*, 89, 1–13.
- Hong, H. P., & Goda, K. (2006). A Comparison of Seismic-Hazard and Risk Deaggregation. *Bulletin of the Seismological Society of America*. <https://doi.org/10.1785/0120050238>
- Idriss, I. M. (2008). An NGA empirical model for estimating the horizontal spectral values generated by shallow crustal earthquakes. *Earthquake Spectra*, 16, 363–372.
- Idriss, I. M. (2014). An NGA-West 2 empirical model for estimating the horizontal spectral values generated by shallow crustal earthquakes. *Earthquake Spectra*. <https://doi.org/10.1193/070613EQS195M>
- IS 1893 (2016) Indian standard criteria for earthquake resistant design of structures, part 1-general provisions and buildings. Bureau of Indian Standards, New Delhi
- Iyengar, R. N., & Ghosh, S. (2004). Microzonation of earthquake hazard in greater Delhi area. *Current Science*, 87, 1193–1202.
- Kanno, T., Narita, A., Morikawa, N., Fujiwara, H., & Fukushima, Y. (2006). A new attenuation relation for strong ground motion in Japan based on recorded data. *Bulletin of the Seismological Society of America*, 96, 879–897.
- Khodaverdian, A., Zafarani, H., Rahimian, M., & Dehnamaki, V. (2016). Seismicity parameters and spatially smoothed seismicity model for Iran. *Bulletin of the Seismological Society of America*. <https://doi.org/10.1785/0120150178>
- Kijko, A. (2004). Estimation of the maximum earthquake magnitude, Mmax. *Pure and Applied Geophysics*, 161, 1655–1681.
- Kijko, A. (2010). Seismic hazard assessment for selected area, Description of MATLAB Code, HA2, 2.05, University of Pretoria, Pretoria, South Africa.
- Kijko, A., & Sellevoll, M. A. (1989). Estimation of earthquake hazard parameters from incomplete data files, part I. Utilization of extreme and complete catalogs with different threshold magnitudes. *Bulletin of the Seismological Society of America*, 79, 645–654.
- Kijko, A., & Sellevoll, M. A. (1992). Estimation of earthquake hazard parameters from incomplete data files, part II. Incorporation of magnitude heterogeneity. *Bulletin of the Seismological Society of America*, 82, 120–134.
- Kolathayar, S., Sitharam, T. G., & Vipin, K. S. (2012). Spatial variation of seismicity parameters across India and adjoining areas. *Natural Hazards*, 60(3), 1365–1379.
- Kulkarni, R. B., Youngs, R. R., & Coppersmith, J. (1984). Assessment of confidence intervals for results of seismic hazard analysis, Proc. of the 8th World Conference on Earthquake Engineering, San Francisco, California, Vol. 1, 263–270.
- Kumar, S., Prakash, B., Manchanda, M. L., Singhvi, A. K., & Srivastava, P. (1996). Holocene landform and land evolution of Indo-Gangetic plain, Uttar Pradesh. Proceedings of a symposium on the NW Himalaya and foredeep, Feb 1995. Geol Surv Spec Publ 21:283–312.
- Lin, P. S., & Lee, C. H. (2008). Ground-Motion Attenuation relationship for subduction-zone earthquakes in Northeastern Taiwan. *Bulletin of the Seismological Society of America*, 98(1), 220–240.
- Marzocchi, W., Taroni, M., & Selva, J. (2015). Accounting for epistemic uncertainty in PSHA: Logic tree and ensemble modeling. *Bulletin of the Seismological Society of America*, 105, 2151–2159.
- Mignan, A., Werner, M., Wiemer, S., Chen, C. C., & Wu, Y. M. (2011). Bayesian estimation of the spatially varying completeness magnitude of earthquake catalogs. *Bulletin of the Seismological Society of America*, 101, 1371–1385.
- Mukhopadhyay, B. (2011). Clusters of moderate size earthquakes along main central thrust (MCT) in Himalaya. *International Journal of Earth Sciences*, 2, 318–325.

- Nath, S. K., & Thingbaijam, K. K. S. (2012). Probabilistic seismic hazard assessment of India. *Seismological Research Letters*, 83, 135–149.
- Nath, S. K., Vyas, M., Pal, I., & Sengupta, P. (2005). A hazard scenario in the Sikkim Himalaya from seismotectonics spectral amplification source parameterization and spectral attenuation laws using strong motion seismometry. *Journal of Geophysical Research*, 110, 1–24.
- Nath, S. K., Raj, A., Thingbaijam, K. K. S., & Kumar, A. (2009). Ground motion synthesis and seismic scenario in Guwahati city, a stochastic approach. *Seismological Research Letters*, 80(2), 233–242.
- Nath, S. K., Mandal, S., Adhikari, M. D., & Maiti, S. K. (2017). A unified earthquake catalogue for South Asia covering the period 1900–2014. *Natural Hazards*, 85, 1787–1810.
- Nath, S. K., Adhikari, M. D., Maiti, S. K., & Ghatak, C. (2019). Earthquake Hazard Potential of Indo-Gangetic Foredeep: its Seismotectonism, Hazard and Damage Modeling for the Cities of Patna, Lucknow and Varanasi. *Journal of Seismology*, 23(4), 725–769.
- NDMA (2010). Development of probabilistic seismic hazard map of India. Technical report by National Disaster Management Authority, Government of India, New Delhi
- Pati, P., Pradhan, R. M., Dash, C., Parkash, B., & Awasthi, A. K. (2015). Terminal fans and the Ganga plain tectonism: A study of neotectonism and segmentation episodes of the Indo-Gangetic foreland basin, India. *Earth-Science Reviews*. <https://doi.org/10.1016/j.earscirev.2015.06.002>
- Prakash, B., Kumar, S., Rao, M. S., Giri, S. C., Kumar, S. C., Gupta, S., & Srivastava, P. (2000). Holocene tectonic movements and stress fields in the western Gangetic plains. *Current Science*, 79, 438–449.
- Rahman, M. M., Bai, L., Khan, N. G., & Guohui, Li. (2018). *Probabilistic Seismic Hazard Assessment for Himalayan-Tibetan Region from Historical and Instrumental Earthquake Catalogs*. Pure Appl: Geophys. <https://doi.org/10.1007/s00024-017-1659-y>
- Rao, M. B. R. (1973). The subsurface geology of the Indo-Gangetic Plains. *Journal of the Geological Society of India*, 14, 217–242.
- Sastri, V. V., Bhandari, L. L., Raju, A. T. R., & Dutta, A. K. (1971). Tectonic framework and subsurface stratigraphy of the Ganga basin. *Journal of the Geological Society of India*, 12, 222–223.
- Scherbaum, F., Delavaud, E., & Riggelsen, C. (2009). Model selection in seismic hazard analysis: An information theoretic perspective. *Bulletin of the Seismological Society of America*, 99, 3234–3247.
- Scordilis, E. M. (2006). Empirical global relations converting MS and mb to moment magnitude. *Journal of Seismology*, 10, 225–236.
- SEISAT. (2000). *Seismotectonic Atlas of India and its environs*. Geological Survey of India.
- Sharma ML, Bungum H (2006) New strong ground motion spectral acceleration relation for the Himalayan region. In First European conference on earthquake engineering and seismology, p 1459
- Singh, R. P., Aman, A., & Prasad, Y. J. J. (1996). Attenuation relations for strong ground motion in the Himalayan region. *Pure and Applied Geophysics*, 147, 161–180.
- Sokolov, V., Zahran, H. M., Youssed, S. E., El-Hadidy, M., & Alraddadi, W. W. (2017). Probabilistic seismic hazard assessment for Saudi Arabia using spatially smoothed seismicity and analysis of hazard uncertainty. *Bull Earthquake Eng*, 15, 2695–2735.
- Sousa ML, Costa AC (2008) Ground motion scenarios consistent with probabilistic seismic hazard deaggregation analysis. Application to Mainland Portugal. DOI <https://doi.org/10.1007/s10518-008-9088-z>
- Spudich, P., Joyner, W. B., Lindh, A. G., Boore, D. M., Margaris, B. M., & Fletcher, J. B. (1999). SEA99: A revised ground motion prediction relation for use in Extensional tectonic regions. *Bull Seism Soc Am*, 89(5), 1156–1170.
- Stein, S., Geller, R. J., & Liu, M. (2012). Why earthquake hazard maps often fail and what to do about it. *Tectonophysics*, 562, 1–25.
- Stepp, J. C. (1972). Analysis of completeness of the earthquake sample in the Puget Sound area and its effect on statistical estimates of earthquake hazard. Proceeding of the International conference on microzonation, vol 2. Seattle, USA, pp 897–910
- Takahashi, T., Saiki, T., Okada, H., Irikura, K., Zhao, J. X., Zhang, J., Thoi, H. K., Somerville, P. G., Fukushima, Y., & Fukushima, Y. (2004). Attenuation models for response spectra derived from Japanese strong-motion records accounting for tectonic source types. 13th world conference of earthquake engineering, Vancouver, B.C., Canada, paper 1271
- Tsapanos, T. M. (2000). The depth distribution of seismicity parameters estimated for the South American area. *Earth Planet Science Letters*, 180, 103–115.
- Uhrhammer, R. A. (1986). Characteristics of northern and central California seismicity. *Earthquake Notes*, 1, 21.
- van Stiphout, T., Zhuang, J., & Marsan, D. (2012). Seismicity declustering, community online resource for statistical seismicity. *Analysis*. <https://doi.org/10.5078/corssa-52382934>
- Virdi, N. S. (1994). The floor of the Tertiary basin of the northwest India – control of basement highs and palaeotopography on the basin evolution. In: Kumar R, Ghosh SK, Phadtare NR (eds) Siwalik foreland basin of Himalaya. *Himalayan Geol* 15:231–244
- Wells, D. L., & Coppersmith, K. J. (1994). New empirical relationships among magnitude, rupture length, rupture width, rupture area, and surface displacement. *Bulletin of the Seismological Society of America*, 4(84), 975–1002.
- Wiemer, S. (2001). A software package to analyze seismicity: ZMAP. *Seismological Research Letters*, 72, 373–382.
- Wiemer, S., & Wyss, M. (2000). Minimum magnitude of completeness in earthquake catalogs: Examples from Alaska, the western United States, and Japan. *Bulletin of the Seismological Society of America*, 90, 859–869.
- Woessner, J., & Wiemer, S. (2005). Assessing the quality of earthquake catalogues: Estimating the magnitude of completeness and its uncertainty. *Bulletin of the Seismological Society of America*, 95, 684–698.
- Youngs, R. R., Chiou, S. J., Silva, W. J., & Humphrey, J. R. (1997). Strong ground motion relationship for subduction earthquakes. *Seismological Research Letters*, 68, 58–73.
- Zhao, J. X., Zhang, J., Asano, A., Ohno, Y., Oouchi, T., Takahashi, T., Ogawa, H., Irikura, K., Thio, H. K., Somerville, P. G., Fukushima, Y., & Fukushima, Y. (2006). Attenuation relations of strong ground motion in Japan using site classification based on predominant period. *Bulletin of the Seismological Society of America*, 96, 898–913.
- Zhao, J. X., Jiang, F., Shi, P., Xing, H., Huang, H., Hou, R., Zhang, Y., Yu, P., Lan, X., Rhoades, D. A., Somerville, P. G., Irikura,

- K., & Fukushima, Y. (2016a). Ground-motion prediction equations for subduction slab earthquakes in Japan using site class and simple geometric attenuation functions. *Bulletin of the Seismological Society of America*, *106*, 1535–1551.
- Zhao, J. X., Liang, X., Jiang, F., Xing, H., Zhu, M., Hou, R., Zhang, Y., Lan, X., Rhoades, D. A., Irikura, K., Fukushima, Y., & Somerville, P. G. (2016b). Ground-motion prediction equations for subduction interface earthquakes in Japan using site class and simple geometric attenuation functions. *Bulletin of the Seismological Society of America*, *106*, 1518–1534.
- Zhao, J. X., Zhou, S., Zhou, J., Zhou, C., Zhang, H., Zhang, Y., Gao, P., Lan, X., Rhoades, D. A., Fukushima, Y., Somerville, P. G., & Irikura, K. (2016c). Ground-motion prediction equations for shallow crustal and upper-mantle earthquakes in Japan using site class and simple geometric attenuation functions. *Bulletin of the Seismological Society of America*, *106*, 1552–1569.

(Received March 15, 2018, revised May 10, 2021, accepted May 15, 2021, Published online May 31, 2021)